EXPERIMENTAL INVESTIGATION AND COMPUTATIONAL FLUID DYNAMICS (CFD) ANALYSIS OF GEOTHERMAL SOURCED HOT AIR DRYING

A Thesis Submitted to
the Graduate School of Engineering and Sciences of
İzmir Institute of Technology
in Partial Fulfilment of the Requirements for the Degree of

MASTER OF SCIENCE

in Energy Engineering

by
Nazlı KELEŞ

September 2022
İZMİR

ACKNOWLEDGEMENTS

I would like to express my sincere gratitude to my supervisor and co-advisor, Prof.Dr. Gülden GOKCEN AKKURT and Asst.Prof.Dr. Hüseyin Utku HELVACI for their guidance and support during my Thesis.

I would like to thank Izmir Institute of Technology for hosting me throughout my education. Special thanks to Prof.Dr. Figen Korel and the Faculty of Food Engineering for allowing me to use the laboratory equipment.

I would also like to thank Assoc.Prof.Dr. Mousa Mohammadpourfard for his guidance and support during the analyzes which are very important to me.

I am grateful to the international research project funded by TUBITAK-NCBR (Project No: 118Y490-POLTUR3/Geo4Food/4/2019). which is played an essential role in tomato cultivation, the installation, and repair of the dryer, in the experimental part of the Thesis and most importantly in purchasing the necessary materials.

I would like to thank my dear friend Meltem Kurnaz, with whom we overcame all the difficulties during the experiments, for being with me and helping me in all the experiments.

I am grateful to İzmir Jeotermal A.Ş. for hosting me during my experiments.

Special thanks to my best friend Selena ALAN for her friendship and support throughout my university life.

Finally, I want to thank my family and my boyfriend for their excellent support, trying to keep me in high spirit throughout the MSc. Programme and never let me give up.

ABSTRACT

EXPERIMENTAL INVESTIGATION AND COMPUTATIONAL FLUID DYNAMICS (CFD) ANALYSIS OF GEOTHERMAL SOURCED HOT AIR DRYING

Drying is one of the oldest methods used to increase the product's shelf life and reduce transportation costs, consisting of heat and mass transfer between the product and the surrounding environment. One of the most common drying methods is hot air drying. The most critical parameters in hot air drying processes are drying air temperature, air velocity and relative humidity.

Renewable energy resources can be used as heat/electricity in drying processes. Geothermal energy resources are highly suitable for hot air drying with their temperature compatibility and reliability. The geothermal resources in Turkey have a high potential for hot air drying.

This Thesis examines tomato slices' quality parameters at different drying air temperatures and velocities. A cabinet-type geothermal sourced hot air dryer is installed in the Yenikale Heat Center of the Balcova-Narlidere Geothermal District Heating System in Izmir-Turkiye. Drying experiments are carried out at 40-60-80°C air temperatures and 0.5-1.5 m/s air velocities to examine their effects on drying kinetics and quality of dried tomatoes, such as pH, color, and moisture. With the help of the data obtained, drying time, drying rate, moisture rate, and effective diffusion coefficients are determined, and dimensionless moisture rate is modeled using thin layer models. Also, energy and exergy analyses are made for each experiment. Finally, experimental and simulation results are compared by using CFD to perform experimental design. The simulations created by using CFD are obtained in a much shorter time and more accurately since all materials used for the experiment are idealized.

ÖZET

JEOTERMAL KAYNAKLI SICAK HAVA KURUTUCUSUNUN DENEYSEL İNCELENMESİ VE HESAPLAMALI AKIŞKANLAR DİNAMİĞİ (HAD) ANALİZİ

Kurutma, ürün ile çevre arasındaki ısı ve kütle transferinden oluşan, ürünün raf ömrünü artırmak ve nakliye maliyetlerini azaltmak için kullanılan en eski yöntemlerden biridir. En yaygın kurutma yöntemlerinden biri sıcak havayla kurutmadır. Sıcak hava kurutma proseslerinde en kritik parametreler, kurutma havası sıcaklığı, hava hızı ve bağıl nemdir.

Yenilenebilir enerji kaynakları, kurutma işlemlerinde ısı/elektrik olarak kullanılabilmektedir. Jeotermal enerji kaynakları, sıcaklık uyumluluğu ve güvenilirliği ile sıcak havayla kurutmaya son derece uygundur. Türkiye'deki jeotermal kaynaklar, sıcak hava kurutma için yüksek bir potansiyele sahiptir.

Bu Tez, domates dilimlerinin kalite parametrelerini farklı kurutma havası sıcaklıklarında ve hızlarında incelemektedir. İzmir-Türkiye Balçova-Narlıdere Jeotermal Merkezi Isıtma Sistemi Yenikale Isı Merkezi'ne kabin tipi jeotermal kaynaklı sıcak hava kurutucusu kuruldu. 40-60-80°C hava sıcaklıklarında ve 0.5-1.5 m/s hava hızlarında kurutma deneyleri yapılarak kurutulmuş domateslerin kurutma kinetiği ve kalitesine pH, renk, nem gibi etkileri incelenmiştir. Elde edilen veriler yardımıyla kuruma süresi, kuruma hızı, nem oranı ve etkin difüzyon katsayıları belirlenmiş ve ince tabaka modelleri kullanılarak boyutsuz nem oranı modellenmiştir. Ayrıca her deney için enerji ve ekserji analizleri yapılmıştır. Son olarak, deneysel tasarımı gerçekleştirmek için CFD kullanılarak deneysel ve simülasyon sonuçları karşılaştırıldı. HAD kullanılarak oluşturulan simülasyonlar, deney için kullanılan tüm materyaller idealize edildiğinden çok daha kısa sürede ve daha doğru bir şekilde elde edilmektedir.

TABLE OF CONTENTS

LIST OF FIGURES

Figure **Page**

Figure **Page**

LIST OF TABLES

Table **Page**

LIST OF SYMBOLS

Symbols

A	Area	m^2
A, B, C	Empirical constants in drying models	-
a_w	Water activity	-
$a*$	Green-red value	-
$b*$	Blue-yellow value	-
C^*	Color intensity	-
c_p	Specific heat	J/kg.K
D_{Eff}	Diffusion coefficient	m^2/s
$\dot{E}x$	Total exergy	kW
h	Enthalpy	kJ/kg
HUE^*	Color vibrancy	-
K, K_0, K_1	Empirical constants in drying models	-
L	Illuminance value	-
$\dot{m}$	Mass flow	kg/s
M	Moisture content	-
MR	Moisture Ratio	-
N	Number of observations	-
P	Pressure	atm
Q	Energy, heat source	kW
R^2	Correlation coefficient	-
s	Entropy	kJ/kg
T	Temperature	°C
t	Drying time	min
V, u	Velocity	m/s
W	Work	kW
Ψ	Specific exergy	kJ/kg
ε	Exergy efficiency	%
λ, λ_{eff}	Thermal conductivity	W/m.K
μ	Dynamic viscosity	pa.s

ρ, ρ_{eff}	Density	kg/m^3
ω	Relative Moisture Ratio	kg_w/kg_{da}

Acronyms

EU	Energy amount	kW
EUR	Energy Usage Rate	%
$RMSE$	Estimated standard error	-
SSE	Standard estimation error	-

Subscripts

cr	Cross section
da	Dry air
Db	Dry bass
dc	Drying Chamber
des	Loss
e	Equilibrium
Eff	Efficiency
Env	Environmental conditions
exp	Experimental
$evap$	Evaporation
fan	Fan
he	Heat Exchanger
i	Initial Moisture Content
ma	Moist air
MWe	Megawatts electric
MWt	Megawatts thermal
o	Dead state
R	Mass flow evaporating from the porous media
pre	Estimated
Sat	Saturated
w	Water

CHAPTER 1

INTRODUCTION

Food is the most basic need of human beings as it provides energy, growth, and repair to the body. Fruits are abundant in the season; they are grown but cannot be consumed out of season. Reducing post-harvest losses is essential to ensure food safety. Agricultural products are classified according to their water content as perishable, semi-perishable, and non-perishable. Drying is the most effective and economical method to preserve foods from spoilage and export them in a quality manner. After a few days of the shelf life of fruits, sensory parameters such as taste, aroma, texture, and color deteriorate, and the fruits become unusable (Source: Iqbal et al., 2019).

Drying is more of a unit process for preserving the fruit, not a chemical process. Its purpose is to stabilize the fruit as biological changes in the fruit cause deterioration. In drying, the moisture in the product is removed up to a certain level; in dehydration, the product reaches bone dryness. Dehumidification is a complex simultaneous heat and mass transfer process. As the product's weight and the area it covers decrease, transportation costs also decrease (Source: Gavrila et al., 2008).

Drying is when moisture is evaporated from the material and swept from the surface, sometimes under vacuum, but typically utilizing carrier gas passing through or through the material. Generally, drying is considered to remove water into a hot stream of air, but drying may involve removing any volatile liquid from any heated gas. For the drying defined in this way to occur, the moist material must obtain heat from the environment by convection, radiation, or conduction or through internal production, such as dielectric or inductive heating; moisture in the body evaporates, and steam is taken up by a carrier gas (Source: Keey, 2011).

The main objectives and advantages of drying are summarized as follows (Source: Sokhansanj and Jayas, 2006);

- A dry food product is less susceptible to spoilage caused by the growth of bacteria, molds, and insects. The activity of many microorganisms and insects is inhibited in an environment where the equilibrium relative moisture ratio is below 70%.

Likewise, the risk of unfavorable oxidative and enzymatic reactions that shorten the shelf life of food is reduced.

- Many favorable qualities and nutritional values of food may be enhanced by drying. Palatability is improved, and likewise, digestibility and metabolic conversions are increased. Drying also changes the color, flavor, and often the appearance of a food item. The acceptance of that change varies by the end user.

- Packaging, handling, and transportation of a dry product are more accessible and cheaper because the weight and volume of a product are less in its dried form. A dry product flows easier than a wet product; thus, gravity forces can be utilized for loading and unloading and short-distance hauling.

- Food products are dried for improved milling, mixing, or segregation. A dry product takes far less energy than a wet product to be milled. A dry product mixes with other materials uniformly and is less sticky than a wet product.

- Drying has also been used as a means of food sanitation. Insects and other microorganisms are destroyed by heat and moisture diffusion.

Although the most common method in the World is still sun drying in the open air, it is not suitable for the contamination of the dried product by dust, soil, and insect factors.Unmanageable drying parameters such as temperature and velocity can cause overdrying, resulting in a reduced quality of the dried product. For this reason, the drying process should be carried out in a closed and controlled environment with hot air in a tunnel or cabinet dryer. As a result of the technical drying process using thermal and electrical energy, it is expected that the quality of the dried products will increase and the drying time will decrease (Source: Garg et al., 2001; Fargali, 2008).

Geothermal energy is a renewable and sustainable resource, and the harm done to the environment is gradually low. It is carbon-free and provides an endless supply of heat. This energy is the affordable solution to reducing fossil-fuel dependency and global warming. The heat procures from beneath the earth's crust.

Direct use of geothermal resources has expanded rapidly in the last 36 years, from space heating of single buildings to district heating, greenhouse heating, industrial

usage, modern balneology, and physical treatment facilities. Geothermal energy utilization capacities in Turkiye at the end of 2021 are shown in Table 1.1.

Table 1.1. Geothermal utilization capacities in Turkiye
(Source: Mertoglu, 2021)

Utilization	**Capacity**
Geothermal district heating (City, residences)	126,000 residences equivalence (1122 MWt)
Greenhouse heating	4.4 Million m^2 (840 MWt)
Heating of thermal facilities, SPAs, thermal hotels and time share facilities	46,400 residences equivalence (420 MWt)
Heat energy of thermal water use in hotels, SPAs and time share facilities	520 Geothermal SPA (1405MWt) (23 Million guests/annual)
Agricultural cooling	4.5 MWt
Geothermal cooling	0.3 MWt
Heat pumps; GSHP	8.5 MWt
Total heat use	~ 3800 MWt (366.000 residences equivalence)
Total electrıcıty productıon	1.7 MWe

In the World, the horticultural industry, especially the fruit industry, is known as one of the high-income parts of the economy of any country. Worldwide 180,766,329 tons of tomato is produced per year. China is the largest tomato producer in the world, with 62,869,502 tons of production per year. India comes second with 19,007,000 tons of yearly production. With 12,841,990 tons of production per year, Turkiye is the third largest producer of tomatoes. China, India, and Turkiye have a share of more than 50% of the World's total tomato production. (Source: FAOSTAT, 2019). The top ten countries in tomato production worldwide are shown in Figure 1.1.

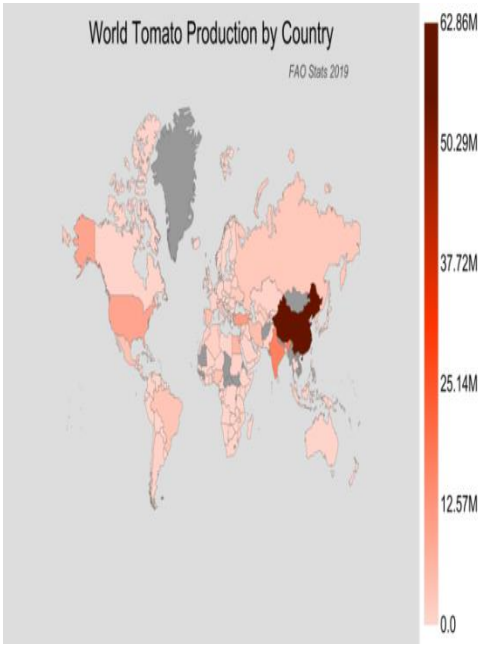

World Tomato Production by Country

	Country	Production (Tons)
	China	62,869,502
	India	19,007,000
	Turkey	12,841,990
	United States of America	10,858,990
	Egypt	6,751,856
	Italy	5,252,690
	Iran	5,248,904
	Spain	5,000,560
	Mexico	4,271,914
	Brazil	3,917,967

Figure 1.1. World tomato production in 2019
(Source: Atlasbig.com)

Tomato is a perishable product that is difficult to transport and preserve due to its high water content and impact sensitivity. For this reason, care should be taken during packaging, transportation, storage, and exhibiting in the market. According to the information compiled from the Southeastern Anatolian Exporters' Associations data, income of tomato export to 51 countries in 2020 is 313,273,000 USD (Source: Carlos, 2022). In 2021, the export exceeded the previous year's figures with a revenue of 363,290, 000 USD. Dried tomato products have a competitive advantage, especially in the foreign market. It is seen that the need for dried vegetables has increased recently, especially in European countries. The USA, which is the country to which Turkiye exports the most, has a large food market (Source: Bashimov, 2016).

Tomato cultivation constitutes one of the essential income sources for Turkish farmers, especially in Marmara, the Mediterranean, the Aegean, and the Black Sea regions. The production in Turkiye, which is 12.84 million tons in 2019, increased by 2.8% to 13.2 million tons in 2020. Antalya is in first place with 2.6 million tons of tomato production (19.5%) in 2020, Bursa is second with 1.3 million tons (10.1%), and Manisa (8.5%) is 1.1 million tons in third place. Tomato is the undisputed and leading product of industrial vegetable growing in Turkiye. Currently, 3.5 million tons (approximately 30%) of the tomato is processed into paste, and 500,000 tons (5%) are

sun-dried and canned (peeled whole, cubed, mashed, etc.). Tomato paste processing facilities in Turkiye have a capacity of 600,000 tons. Due to the climate advantage, sun-dried tomatoes have great potential, and almost all (97%) production is exported. There is also a small amount of tomato juice and sauce production (Source: Abak, 2010).

As seen in Table 1.2, tomato production and consumption capacity is approximately constant from 2015 to 2020 (excluding 2018/19). However, there is a decrease in production in 2018/19, so the amount of imported tomatoes is quite high compared to other years.

Table 1.2. Turkiye tomato data (thousand tons)
(Source: TUIK 2021)

	2015/16	**2016/17**	**2017/18**	**2018/19**	**2019/20**
Production	12615	12600	12750	12150	12842
Consumption	9340	9284	9443	9013	9511
Import	10.9	10.4	11.2	34.8	17.4
Export	1195	1246	1205	1155	1220

Dried tomatoes (Figure 1.2) are a valuable source of minerals such as magnesium, potassium, and calcium. All these minerals play an essential role in the functioning of the heart muscles, creating electrolyte balance, healthy bone tissue in the body, and energy production. It is also essential for cleansing the liver. Dried tomatoes are also rich in vitamins A, K, and C. While vitamin K is significant for blood clotting, vitamin B triggers brain development to a great extent. Dried tomatoes have excellent effects on both the immune system and eyesight, and are very rich in cancer-fighting antioxidants. It is a source of Lycopene, one of the powerful antioxidants, and it fights against cancerous cells in particular. Dried tomatoes meet a significant part of the daily iron need with their iron content. In addition, the potassium content of dried tomatoes prevents high blood pressure or lowers blood pressure (Source: Saygi, 2019).

Figure 1.2. Dried tomatoes
(Source: Demiray et. al., 2008)

Computational Fluid Dynamics (CFD) is a branch of fluid mechanics in which problems involving fluid behavior are analyzed by solving problems using numerical methods and algorithms. CFD, as a developing application, has started to attract attention from international circles with the advances in digital computers. Since the late 1960s, there has been remarkable growth in the applications of CFD. And it has become an essential part of engineering design and analysis, as it allows for developing new designs and estimating the performance of processes before they are implemented. Today, researchers, equipment designers, and process engineers; widely use CFD to analyze the performances and flows of furnaces, cooling cabinets, stirred boilers, spray dryers, heat exchangers, and other process equipment. In design and development, CFD programs are not only concerned with fluid behavior but also heat and mass transfer (evaporation or dissolution, etc.), phase change (freezing, melting or boiling, etc.), and chemical reactions (burning or rusting, etc.), They are standard numerical tools that also deal with issues such as mechanical motion (rotation of agitator, pistons, fans, etc.) and stress or deformation in solids (Source: Kaushal, 2012).

The drying rate is a function of air velocity or air temperature. Therefore, it is essential to know the air temperature and velocity in a drying environment. However, these parameters can be challenging to measure during operation, as many sensors are required that must be positioned at different locations in the air velocity, making this even more complicated when there is turbulence. At this point, CFD can be beneficial in defining the drying process (Source: Süfer et al., 2016).

Balçova-Narlıdere Geothermal District Heating System (BNGDHS) is installed in 1996, providing heating and domestic hot water to the buildings. It is located 7 km west of İzmir city center and 1 km south of the İzmir-Çeşme highway and is the largest geothermal district heating system of Turkiye. The facilities of the BNGDHS are 13 heat centers, 2 (reinjection) pumping stations, 13 production wells, 5 reinjection wells, 4 observation wells and a total of 460 km pipeline (Source: Izmir Geothermal Inc., 2021). The schematic diagram of the system is shown in Figure 1.3. Geothermal fluid drawn by production wells at a flowrate of 597 kg/s and a temperature of 110-120°C. The fluid transfers its heat to clean city water through heat exchangers at heat centers, and reinjected back to the reservoir at 55-60°C. The clean city water (70-85°C) circulates through the city, transfers its heat to another heat exchangers located at the buildings, then returns back to the heat centers (50-55°C). In summer time. Heat is needed only for domestic hot water supply (EBRD, 2020).

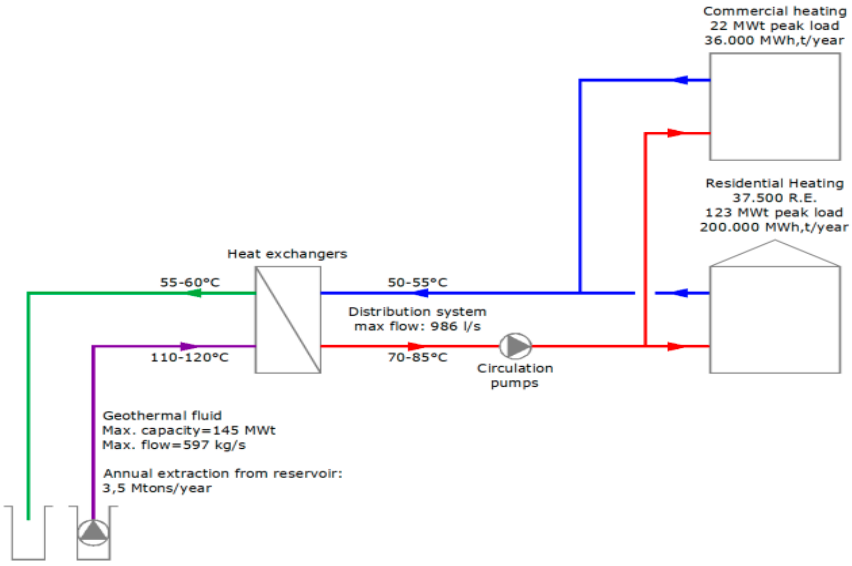

Figure 1.3. Schematical diagram of BNGDHS system

Thesis consists of two parts. In the first part, a geothermal-sourced cabinet-type hot air dryer is used to dry tomatoes in one of the heat centers of BNGDHS. The drying experiments are conducted in the summer season using clean city water returns from the building heat exchangers. Since summertime geothermal resources are used only for domestic hot water heating, clean city water return temperature is 80-85°C which is enough for drying experiments. The second part models and analyzes the dryer and tomato slices using a CFD tool. The primary purpose of drying processes is to determine the effective drying parameters of tomatoes by pH analysis, color analysis,

and moisture determination and to examine the effects of these parameters on drying kinetics. The objectives of the experimental results validate the model, and the simulations evaluate and improve the drying procedure.

The Thesis includes 6 chapters. In Chapter 2, drying principles and drying mechanisms are explained. Also, dryers and drying methods are summarized. Chapter 3 presents a literature review, including previous studies on tomato drying kinetics. In Chapter 4, the test unit and test procedure are given. Quality parameters of dried tomatoes are defined, and the evaluation of drying energy performance and exergy analysis methods are also presented in Chapter 4. Chapter 5 discusses the drying properties of tomatoes, the quality of dried tomatoes, and the results from experiments for energy and exergy analyses. Finally, the results are outlined in Chapter 6.

CHAPTER 2

DRYING

Drying can be defined as the evaporation and removal of water or other liquids from a solution, suspension, or other solid-liquid mixture to form a dry solid. There are various factors that influence the drying process. These factors include heat, dew point temperature, drying time, air velocity, drying material type, state and quantity (Source: Treco.co.uk). Drying is a complex process involving simultaneous heat and mass transfer accompanied by physicochemical transformations. It is expected that many different drying types will be used in an industry that is as diversified and widespread as the food industry. The followings are some general methods of drying:

- The first one is the application of hot air (convective or direct drying). Hot air drying is the most common commercial method for drying vegetables and fruits. During drying, the convective air flow passes over the product's surface(Source: Lee et al., 2016). Figure 2.1 illustrates the convective drying process. Heat and mass transfer are critical in drying processes. In order to evaporate the liquid in the material intended to be dried, heat is transferred to the product and evaporation occurs after the temperature of the liquid reaches the evaporation level. The evaporated liquid mass is transferred to the air surrounding the material. The two parameters required for this process are air temperature and velocity. As the drying air temperature increases, its moisture-holding capacity also increases (Source: Parikh, 2014).

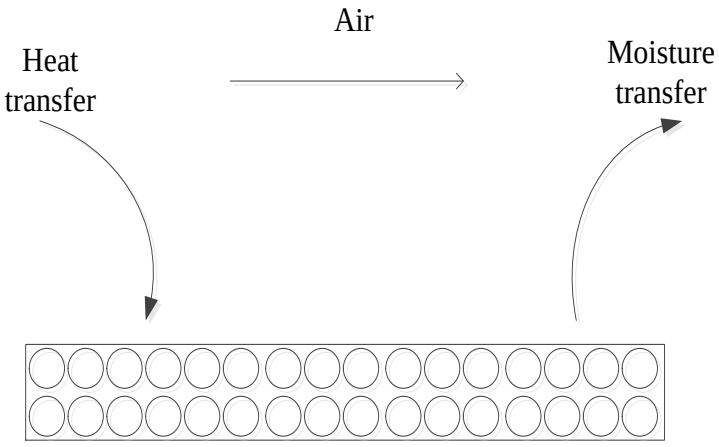

Figure 2.1. Convective drying process

(Source: Ozler et.al., 2011)

- In conductive drying, the heated surface is in contact with the material, and necessary precautions should be taken to prevent the material from overheating and to ensure that the heating is homogeneous. Conductive drying is also widely used in the drying and producing paper products (Source: Li et.al., 2013). However, conductive drying may encounter problems such as being unable to reach high drying rates, non-uniform heat and mass transfer conditions, control problems, and high investment and operating costs.

- Electromagnetic radiation is used in ultraviolet drying. Monomeric coatings and dyestuffs are processed by drying under the influence of UV radiation. The biggest problem in applying ultraviolet drying is the high investment cost (Source: Faith, 2001).

- Freeze drying can be applied in the production of pharmacological products, serums, bacterial cultures, fruit juices, vegetables, coffee and tea extracts, and meat and milk production. The material is first frozen. The high vacuum associated with the chemical dehumidifier or low-temperature condenser is then taken to the applied volume. Heat transfer is provided to the frozen material by conduction or infrared radiation. Meanwhile, the volatile element is usually water sublimated and condensed or absorbed by the desiccant. Freeze drying is generally applied between -10 °C and -40 °C. Freeze drying is an expensive and slow process, suitable for heat-sensitive materials (Source: Ahmed et.al., 2013).

- Supercritical drying (superheated steam drying) involves steam drying of products containing water. This process is feasible because the water in the product is boiled off and joined with the drying medium, increasing its flow. The process has the potential for use in foods if carried out at reduced pressure, to lower the boiling point (Source: Romdhanaa et.al., 2015).

- Natural air drying occurs when materials are dried with unheated forced air, taking advantage of its natural drying potential. The process is slow and weather-dependent, so a wise strategy, "fan off-fan on," must be devised considering the following parameters: Air temperature, relative moisture ratio, moisture content, and temperature of the drying material (Source: Ahmed et.al., 2013).

In drying, it is necessary to remove free moisture from the surface and also moisture from the interior of the material (Figure 2.2). Water is held on the surface by many forces, from rigid chemical bonds to brittle forces. The water that is most easily removed during drying is the loosely held water, so the free water on the surface evaporates more easily than the water in the material. The water in the inner layers evaporates much more slowly, and the process is more complex than in the outer layers. (Source: Earle, 1983)

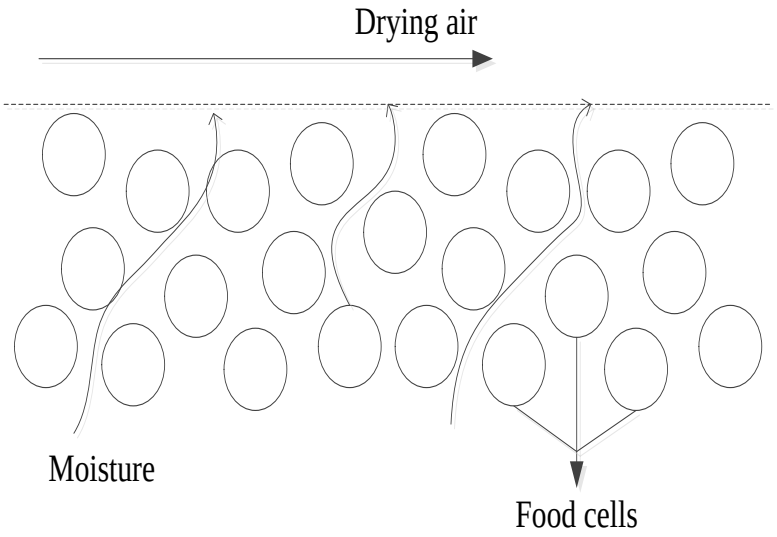

Figure 2.2. Schematic representation of the drying process
(Source: Zaini, 2010)

If the change in moisture content of material is determined as a function of time, a smooth curve is obtained from which the drying rate at any given moisture content may be evaluated. Drying usually follows two separate drying zones; the constant rate period and the falling rate period. The two zones are separated by a breaking point called critical moisture content. Figure 2.3 shows a typical drying rate curve for constant drying conditions. Drying rate experiments can be conducted by measuring the weight change of the drying material during the drying process (Source: Geankoplis, 2003, Fellows 2009).

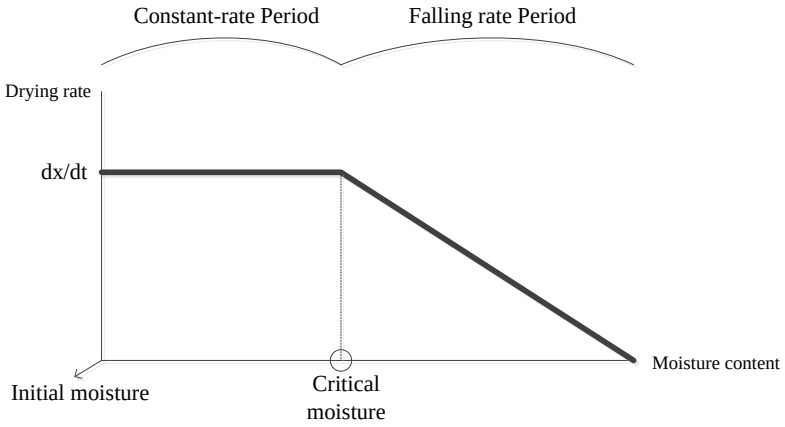

Figure 2.3. Drying rate versus moisture content
(Source: Traub, 2002)

In the constant rate period, heat transferred from the drying air to the material becomes equal to the evaporation rate. The drying rate is determined by the difference between the water content on the material's surface and the drying air's water content.

During the constant rate period, it is assumed that drying occurs from a saturated surface of the material by diffusion of the water vapor through a stationary air film into the air stream. The behavior in which the drying behaves as though the water are at a free surface is called constant rate drying (Source: Treybal, 1981). If x is the mass of the material being dried at the beginning of the process and t is the mass of the material being dried at time t, then the drying rate is expressed by Equation 2.1. The drying rate is constant for the constant-rate period.

$$\frac{dx}{dt} = \text{constant} \qquad (-) \qquad (2.1)$$

While the drying continues at a constant rate, when the moisture content decreases, the moisture inside the particle can not diffuse to the outer surface to form a continuous liquid film because the moisture content of the material decreases due to drying. On the dried outer surface, dry spots begin to form from place to place. Thus, starting from the critical moisture content point, the drying rate starts to decrease, and the surface temperature of the material begins to increase. Afterward, the dry spots multiply and enlarge, forming a dry outer layer. The drying rate decreases continuously with the formation of a dry layer with low heat permeability and the decrease in the diffusion rate of the liquid layer to be carried to the surface. This part of drying is called the falling rate period (Source: Lee, 1994).

CHAPTER 3

LITERATURE REVIEW

Drying is the oldest method of preserving food. Throughout history, the sun, the wind and a smoky fire are used to remove water from fruits, meats, grains and herbs. Traditional open sun drying is the most popular food-reservation technique to the local farmers due to near-zero capital cost and cheap labor cost. However, this method is highly energy intensive, unhygienic, and time demanding. For this reason, hot air drying processes are more advantageous in terms of both energy and time in drying processes. It is more hygienic as it takes place in a closed environment. In fruit and vegetable drying processes, the hot air drying process is generally preferred. The purpose of drying fruits and vegetables is to prolong storage, reduce the need for packaging and decrease the weight during transportation. Drying is the best way to maintain nutritional value at the optimal level.

Tomatoes are the products that are consumed all around the year as fresh and dried. The demand for dried tomatoes is increasing in the World.

The time required to dry the tomatoes depends on tomato variety and size, air temperature,relative humidity and velocity, thickness of the tomato slices, loading on the tray, pre-treatment of the fresh fruits and efficiency of the dryer (Source: Kostoglou et. al., 2013).

Andritsos et al. (2003) explain that ideal conditions for drying tomatoes are mild temperatures between 45 and 55°C, which allow the dried product to retain its nutrients (including vitamins and lycopene, which are responsible for the deep red color of tomatoes) and aromas. Another study conducted by Kostoglu (2013) concluded that drying of tomatoes at 80°C and above resulted in a hardened surface and the occurrence of severe oxidative damage.

Conventional energy sources such as coal, natural gas, and electricity are used for the heat energy required for drying. Due to the increase in cost and pollution involved in conventional sources, renewable energy sourced drying systems can be encouraged.

Başak et. al. (2014) identified geothermal and solar energy as renewable sources in agricultural product drying processes. The daily and seasonal variability of solar energy negatively affects the drying process, which is the main disadvantage of using solar energy. Geothermal energy is a continuous source which does not change daily between day and night and seasons. While geothermal fluid as a heat source, can be used to heat air through a heat exchanger for hot air dryers, electrical power is only used to run the fan of the drier and pumps for geothermal fluid circulation. The most extensive geothermal drying facilities are located in New Zealand and deal with the drying of alfalfa, timber, and pulp (Source: Kostoglou et al., 2013). Basak et al. (2014) declared that the geothermal resources in Turkey are suitable for fruit and vegetable drying processes in terms of temperature. Vegetables that are dried and packaged with modern techniques can be marketed all over our country. After the demand from the Turkish market is met, it is possible to export it to European Union Countries and Middle East countries (Source: Ozler et al., 2004).

Drying fruits and vegetables is a complex operation that demands much energy and time. Dependence purely on experimental drying practices, without mathematical considerations of the drying kinetics, can significantly affect the efficiency of dryers, increase the cost of production, and reduce the quality of the dried product. Thus, the use of mathematical models in estimating the drying kinetics, the behavior, and the energy needed to dry agricultural and food products becomes indispensable (Source: Onwude, 2016).

To evaluate and select the appropriate drying curve equation, 10 different models are used. These models are Newton, Page, Logarithmic, Two term, Henderson & Pabis, Modified Page, Wang & Shing, Modified Handerson & Pabis, Approximation of diffusion, Midilli et. al.. The models are compared according to three statistical parameters; such as root mean square error (RMSE), chi-square (X^2) , and coefficient of determination (R^2). The R^2 is a number between 0 and 1 that measures how a product in a statistical model predicts an outcome. In an analogy to standard deviation, for an unbiased estimator, the RMSE is the square root of the variance, known as the standard error. Also, the X^2 is a test that measures how a model compares to actual observed data.

The mathematical formulation of mass transfer in drying processes is often based on the diffusion equation. In principle, the diffusion coefficient as a function of moisture content has to be determined experimentally (Source: Yagcıoglu, 2007).

Bagheri et. al. (2013) applied 9 different thin-layer drying models to explain the drying behavior of tomato slices and they compared the models with experimental data by R^2, RMSE, and X^2 values. As a result of the experiments conducted by Akhijani et al. (2016) and Bagheri et al. (2013), it is determined that the most suitable thin layer model is the Page model by looking at the values where R^2 is the highest; X^2 and RMSE are the lowest. Also, Akhijani et al. (2016) reported that the effective moisture diffusion for tomato slices ranged from 1.58×10^{-9} to 6.98×10^{-9} m^2/s.

Taheri-Garavand et al. (2011), on the other hand, states that Midilli et al. gives the best results among these models, according to the statistical analyzes applied to all models.

Purkayastha et al. (2011) showed that effective moisture diffusion values ranged from 0.545×10^{-9} to 2.387×10^{-9} m^2/s. Under the evaluated experimental conditions, the model that best represents the drying kinetics of blanched tomato slices is the Logarithmic model, followed closely by the Henderson-Pabis model. Some researchers have also reported that the Logarithmic model adequately predicts thin-layer drying of various agricultural products (Source: Doymaz, 2008; Khazaei and Daneshmandi, 2007; Midilli and Küçük, 2003).

Hussein et al. (2016) determined that the D_{eff} values obtained for tomato slices should be in a specific range. It is generally 10^{-12} to 10^{-8} m^2/s for drying agricultural materials (Source: Doymaz, 2010). In addition, Sacilik et al. (2006) for available sun-dried tomato slices (1.31×10^{-9} m^2/h); Akanbi and Adeyemi (2006) for tomatoes dried at 45°C to 75°C ($3.72\text{-}12.27 \times 10^{-9}$ m^2/h) and Doymaz (2007) for tomatoes dried at 55°C to 70°C ($3.91\text{-}7.53 \times 10^{-10}$ m^2/s). The practical moisture diffusion values are $2.00\text{-}5.84 \times 10^{-10}$ m^2/s in hybrid dried tomato slices and $1.37\text{-}4.40 \times 10^{-10}$ m^2/s, and $1.33\text{-}4.01 \times 10^{-10}$ m^2/s in open sun-dried tomato slices of 4 to 8 mm thickness.

Drying includes solving a series of heat and mass transfer equations such as heat and moisture exchange between product and air, adsorption and desorption rates of heat and moisture transfer, equilibrium relations between product and air, and psychometric

properties of moist air. The nonlinear system of partial differential equations can be solved by the Comsol Multiphysics software with a predefined set of initial and boundary conditions (Source: Gavrila et al., 2008).

Mathioulakis et al. (1998) simulated air movements in a batch-type industrial tray dryer. It has been emphasized that drying tests of many fruits vary depending on the positions in the dryer. The results obtained by determining the pressure and air profiles by CFD revealed that the differences in drying rates and moisture contents are due to the inhomogeneous distribution of the air in the dryer. Mirade and Daudin (2000) used CFD technology to access data on the air movement in a sausage dryer in their study. When they compared the measurement data with the data obtained from the model, they found differences between the air velocities.

In this Thesis tomato drying experiments (X^2) is carried out in a geothermal sourced cabinet dryer. Drying kinetics are investigated with different drying air temperatures and velocities; quality parameters such as pH, color and moisture of dried tomatoes are determined. During the experiment; Drying time, temperature, RH and velocity is measured and drying rate and effective diffusion coefficients are determined and moisture ratio is modeled using thin layer models. In addition, Comsol Multiphysics is used for CFD analysis of air and dried material inside the dryer.

.

CHAPTER 4

MATERIALS AND METHODS

In this thesis, these experiments aimed to examine the effects of drying air temperature and speed on dried tomatoes. In addition, the quality parameters of the dried tomatoes are examined and the diffusion coefficients are calculated. Their compatibility with thin layer models is checked. Finally, it is modeled with Comsol Multiphysics software and the experimental results and simulation results are validated.

Albeni types tomatoes which are dried in a geothermal sourced cabinet type dryer, are grown in the backyard of Yenikale Heat Center (Figure 4.1). It is a hybrid industrial tomato variety that is recommended for the Aegean, Marmara, Thrace, and other regions where industrial tomatoes are produced. The fruits are egg-shaped, long conical, red in color, with a hard shell. The plant structure is solid; the leaves are large and fleshy with a weight range of 95-110 gr (Figure 4.2).

Figure 4.1. Tomato cultivation area

Figure 4.2. Albeni type tomatoes
(Source: SunagriTohumculuk.com)

A geothermal sourced cabinet type drier is installed to Yenikale Heat Center, is shown schematically in Figure 4.3. The geothermal dryer consists of a fan section and a drying chamber section. The inner surface of the dryer is insulated with fiberglass and covered with an aluminum sheet to reduce heat losses. Fan section consists of a centrifugal fan (1) and a heat exchanger (2). After the geothermal fluid is drawn from underground and sent to the surrounding buildings for district heating purposes, it returns to the heat center. It enters the heat exchanger of the geothermal dryer (13) at a temperature of 80-85°C.

On the other hand, ambient air is drawn by a centrifugal fan, passes over a heat exchanger where a geothermal fluid circulates, increases its temperature, and reaches the drying chamber section. This section has six trays (3), and an air circulation unit (5) is available to recycle the exhaust air. The air temperature can be regulated by changing the flow rate of the geothermal fluid while the air velocity can be changed by the control unit of the fan. A ball valve changes the geothermal fluid flow rate. The dryer specifications are given in Table 4.1.

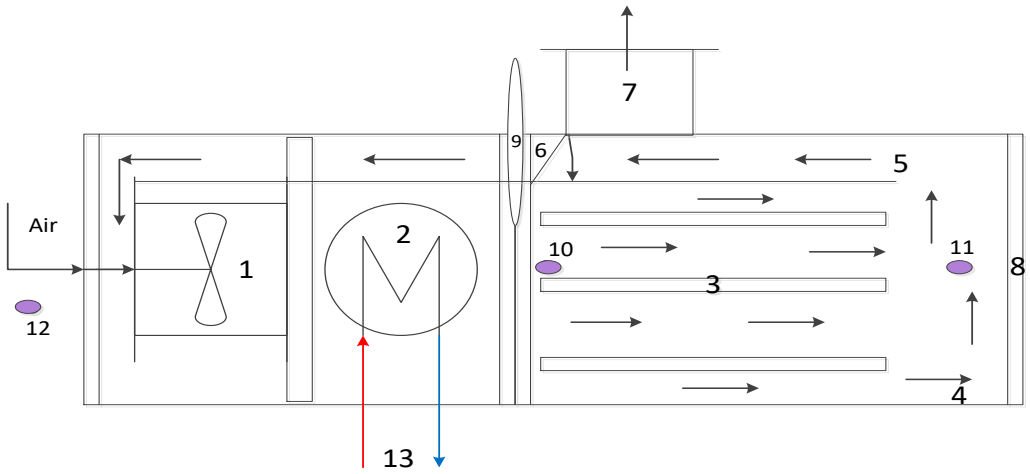

Figure 4.3. Schematic representation of the geothermal dryer

Respectively, the types of equipment included in the schematic representation of the geothermal dryer in Figure 4.3 are: Fan (1) is to overcome the aerodynamic resistance in the dryer, appropriate fan selection should be made according to the air velocity, mass, and pressure of the dryer air. Hot air can circulate around the trays loaded with tomatoes by installing radial fan units in the system. Heat exchanger (2) is a device used to transfer thermal energy (enthalpy) between two or more fluids, between a solid surface and a fluid, or between solid particles and a fluid, at different temperatures in thermal contact. Heated air is brought into contact with the product in a

closed area to facilitate dehydration. Trays (3) or similar product holders expose this product to hot air. The essential part where the material is dried is the rectangular section drying room (4). It is the part that remains constant throughout drying. Loading-unloading is done from only one side of the room. It is the section with trays inside. Recirculation unit is shown as number 5. The drying products are heated using geothermal water. After some moisture content has condensed, the air from the dryer is recirculated. The main advantage of recirculating air is that the moisture ratio and air temperature can be controlled by utilizing cold water in an air condenser. Discharge flap (6) is a section with a winged structure located above the drying chamber. Wing angles are adjusted with the help of a lever. Chimney (7) allows the hot air from the discharge flap to mix with the atmosphere. Cover (8) is to prevent heat loss and avoid external effects, covers that cut the contact of the drying chamber with the outside are used. Anemometer (9) is the sensor used to measure the air velocity of the air-liquid passing through the drying chamber for drying the materials. Thermocouples (10-11-12) are a temperature sensor. It consists of two different conductive materials. The temperature difference between the hot and cold spots creates a voltage on the thermocouple. Geothermal fluid inlet-outlet line (13) is the inlet and outlet section of geothermal water for drying in the tomato drying process.

The procedure to be followed during experiments is given below, according to Figure 4.2.

First of all, the precision balance is reset. The tray (3) is placed on the support frame. After the preparation, the initial value is read and saved on the balance. The tomatoes to be dried are sliced and spread in a thin layer on the tray. The tray is placed on the support frame, and the total weight is recorded. The tray is placed in the drying chamber (4), and the cover is closed (8). The fan (1) is turned on, and the speed is adjusted. The valves in the inlet-outlet lines (13) of the geothermal fluid are opened. The velocity of the fluid circulating in the drying chamber is measured with an anemometer (9), and the value is recorded. The heat exchanger (2) valves are opened, and the temperature is adjusted. Temperature values at different points of the drying chamber are controlled with thermocouples (10-11-12). The drying test time measurement is started with a stopwatch. The mass of the tomato is measured every 15 minutes for the first 1 hour, every 30 minutes for the next 2 hours, and then hourly until the humidity value reaches 8-12%. The heat exchanger inlet-outlet valves are closed, and the fan section is kept waiting for cooling thanks to the chimney (7). After 15

minutes, the trays are removed. The appliance is switched off after the fan is turned off and the drying process ends. Samples are taken from dried tomatoes, placed in ziplock bags, and stored for analysis, such as pH, color, and moisture determination.

Table 4.1. Features of geothermal source cabinet type dryer

Height of dryer	(mm)	554
Width of the dryer	(mm)	1100
Length of dryer	(mm)	2000
The width of the tray	(mm)	500
Length of tray	(mm)	600
Thickness of each tray	(mm)	20
Distance between trays	(mm)	100
Area of circulation unit	(mm)	210
Height of the tray from the ground	(mm)	720
Critical area of the dryer	(m^2)	0.3474
Number of trays		6

Pre-installation images of the dryer are given in Figure 4.4. The dryer is installed inside the heat center by a technical team of Izmir Geothermal Inc. (Figure 4.5 and Figure 4.6). Geothermal fluid inlet-exit line connections to the heat exchanger can be seen in Fig.s 4.6-4.8. Control valves are installed at both ends of the pipeline to control the geothermal fluid flow and adjust the cabinet temperature. An electrical panel is connected for the fan speed control. A mechanical manometer, thermometer, and calorimeter are installed on both inlet and outlet lines to measure the geothermal fluid's temperature, pressure, and velocity (Figure 4.7).

Figure 4.4. The state of the dryer before it is installed

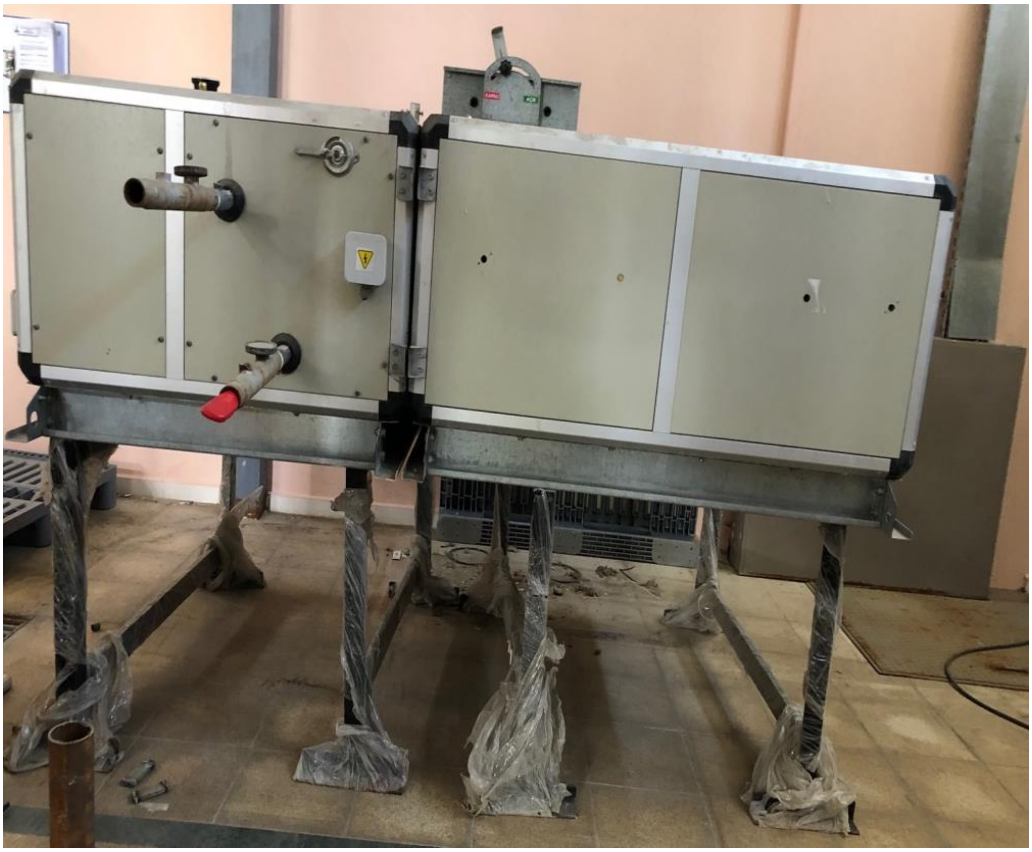

Figure 4.5. The feet of the dryer are mounted and the cabinets are connected to each other

Figure 4.6. Connection of input and output lines

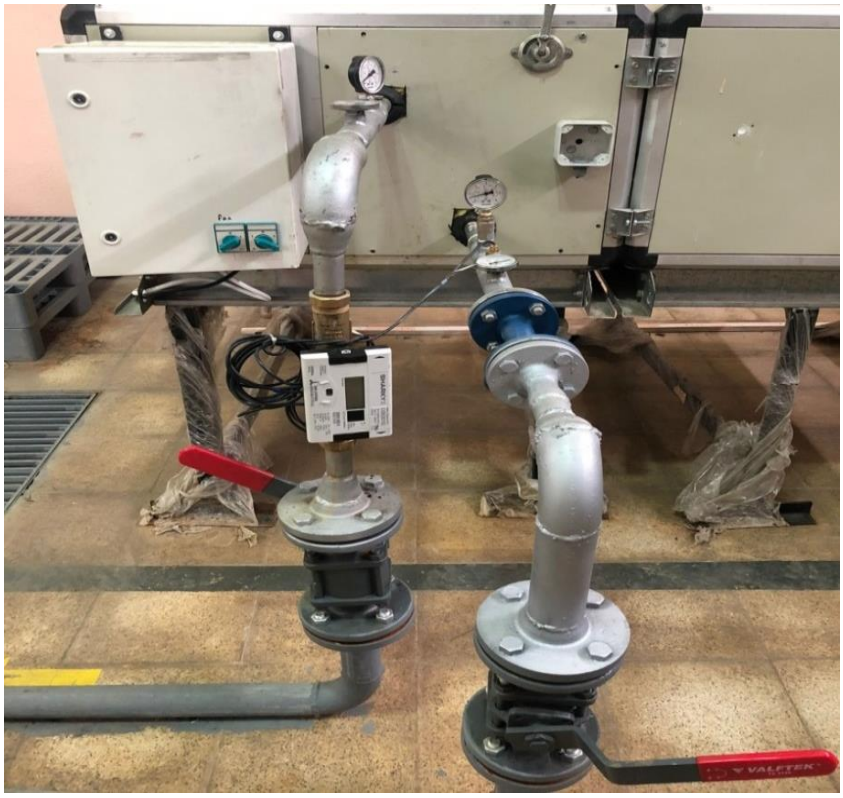

Figure 4.7. The inlet-outlet line of the geothermal fluid to the dryer

Figure 4.8. Dryer-geothermal line connection

4.1 Determination of Moisture Content, Moisture Ratio and Drying Rate

Moisture content

Moisture content is determined by subtracting the initial mass from the final mass and dividing by the initial mass of the wet product in Equation 4.1 (Source: Appoldt and Raihani, 2017).

$$Moisture\ Content\ (M) = \frac{\text{Initial mass} - \text{Current mass}}{\text{Initial mass}} * 100 \quad (\%) \qquad (4.1)$$

Moisture ratio

In order to calculate the moisture ratio, several consecutive operations are performed. First, the instant moisture ratio is calculated according to Equation 4.2.

$$\text{Instant Moisture Ratio} = \frac{[((m_i - m_t)/m_i) * 100]}{\text{Moisture content}_i} \quad (-) \qquad (4.2)$$

m_i and m_t are the sample's initial and instantaneous mass measurements, respectively. The moisture content is the initial moisture content calculated for each sample.

The moisture ratio is calculated with Equation 4.3.

$$\text{Moisture Ratio} = \frac{\text{Instant Moisture Ratio}}{\text{Moisture Ratio}_i} \quad (-) \qquad (4.3)$$

Drying rate

The moisture content change in the dried product per unit of time is called the "drying rate" and is calculated according to Equation 4.4.

$$\text{Drying Rate} = \frac{\text{Instant Moisture Ratio}}{\Delta t} \quad \left(\frac{\text{g water}}{\text{g dry matter.min}}\right) \qquad (4.4)$$

Before starting the experiments, a slice of tomato is sampled and weighed to determine the initial moisture content of tomatoes. Then the slices are placed on trays and placed in the dryer (Figure 4.9). Tomatoes are left to dry at constant air temperatures and velocities until they reach a constant weight. Then, the moisture content is calculated according to Equation 4.1.

Drying experiments are carried out in August-September 2021 at three different drying air temperatures of 40-60-80°C and two different drying air velocities of 0.5-1.5 m/s (Table 4.2).

Figure 4.9. Arrangement of tomato slices on the tray

Table 4.2. Experiment conditions

Temperature (°C)	**Air velocity (m/s)**
40	0.5
	1.5
60	0.5
	1.5
80	0.5
	1.5

4.2 Thin Layer Drying Models

Thin layer drying means drying the sample particles or slices in a single layer (Source: Midilli et al., 2002). Thin layer equations have been included in many drying studies in recent years. This is due to ease of use and little data set. The formulas of the thin layer drying models consist of the MR equation, so in order to obtain results about the thin layer drying models, the MR must be calculated first. The moisture ratio (MR) of tomatoes during drying experiments is calculated using Equation 4.5 (Source: Purkayastha et al., 2013).

$$MR = \frac{M - M_e}{M_i - M_e} \qquad (-) \qquad (4.5)$$

Equation 4.5 has been simplified to Equation 4.6 because the M_e values are minimal compared to the M or M_i values.

$$MR = \frac{M}{M_i} \qquad (-) \qquad (4.6)$$

The thin layer models commonly used for tomato drying are listed in Table 4.3. Since the MR values are known for each experiment, the coefficients in the equations need to be calculated. The coefficients in these models are determined by performing nonlinear regression analysis. In addition, some parameters are calculated using MR to determine the most suitable model. These; coefficient of determination (R2), standard error of estimation (SSE), and estimated standard error (RMSE). These parameters are given in Equations 4.7, 4.8 and 4.9, respectively (Source: Taheri-Garavand et al., 2011). The thin layer model, where the R^2 value is closest to one, but the RMSE and SSE values are closest to zero, is the best fit for the experimental model.

Table 4.3. Thin layer drying models

Name of Model	**Equation of Model**	**Reference**
Newton	MR= exp(-k*t)	Tunde-Akintunde and Oke (2012)
Page	MR= exp(-k*(t^n))	Hassan-Beygi et.al. (2009)
Modified Page	MR= exp(-(k*t)^n)	Hayaloglu et.al.. (2007)
Henderson &Pabis	MR= a*exp(-k*t)	Shittu and Raji (2011)
Logarithmic	MR= a*exp(-k*t)+c	Tunde-Akintunde and Oke (2012)
Two term	MR= a*exp(-k_0*t)+b*exp(-k_1*t)	Dandamrongrak et.al.. (2002)
Approximation of diffusion	MR= a*exp(-k*t)+(1-a)* exp(-k*a*t)	Hayaloglu et.al.. (2007)
Wang & Singh	MR=1+a*t+b*(t^2)	Çelen et.al.. (2013)
Modified Henderson&Pabis	MR= a*exp(-k*t)+b* exp (-g*t)+c*exp(-h*t)	Karathanos (1999)
Midilli et.al.	MR= a*exp(-k*(t^n))+b*t	Midilli et.al.. (2002)

$$R^2 = 1 - \left[\frac{\sum_{i=1}^{N}\left(MR_{per,i} - MR_{exp,i}\right)^2}{\sum_{i=1}^{N}\left(\overline{MR_{per,i}} - MR_{exp,i}\right)^2}\right] \qquad (-) \qquad (4.7)$$

$$SSE = \frac{\sum_{i=1}^{n}\left(MR_{exp,i} - MR_{pre,i}\right)^2}{N} \qquad (-) \qquad (4.8)$$

$$RMSE = \left[\frac{1}{N}\sum_{i=1}^{n}\left(MR_{exp,i} - MR_{pre,i}\right)\right]^{\frac{1}{2}} \qquad (-) \qquad (4.9)$$

4.3 Determination of Diffusion Coefficient

The diffusion coefficient is determined by minimizing the gap between the experimental and simulated curves. The drying effects of the products in the falling rate period can be explained using the Fick diffusion equation. The solution of the Fick equation for products with sheet geometry is shown in Equation 4.10 (Source: Hussein et al., 2016).

$$MR = \frac{8}{\pi^2}\sum_{n=0}^{\infty}\frac{1}{(2n+1)^2}\exp\left(-\frac{(2n+1)^2\pi^2 D_{eff}t}{4L^2}\right) \qquad (-) \qquad (4.10)$$

Equation 4.10 can be simplified to Equation 4.11 by considering only the first term of the series solution. Taking the natural logarithm of both sides of the equation gives a linear function (Equation 4.12).

$$MR = \frac{8}{\pi^2}\exp\left(-\frac{\pi^2 D_{eff}t}{4L^2}\right) \qquad (-) \qquad (4.11)$$

$$\ln(MR) = \ln\frac{8}{\pi^2} - \frac{\pi^2 D_{eff}t}{4L^2} \qquad (-) \qquad (4.12)$$

Accordingly, the diffusion coefficient (Deff) can be obtained from the slope of the lnMR plot against the drying time (t) (Equation 4.13).

$$Slope = \frac{\pi^2 D_{eff}}{4L^2} \qquad (-) \qquad (4.13)$$

4.4 Quality Parameters

The success of the tomato drying process is determined by quality parameters such as pH, color and moisture content. pH and color analysis are applied to wet and dried tomatoes while moisture content is determined only for dried products.

4.4.1 pH Analysis

Milwaukee MW102 pH meter is used for the pH analysis of wet and dried tomatoes (Figure 4.10). The MW102 is a microprocessor-based pH and temperature meter with an extended range, automatic temperature compensation, 2-point automatic calibration, and pH accuracy of ±0.02. The features of the device are given in Table 4.4.

Table 4.4. Milwaukee MW102 specifications

(Source: Milwaukeeinstruments.com)

Model		**Milwaukee MW102**
pH range		-2 ÷ 16
Temperature range	(°C)	-5 ÷ 70
Resolution (pH)		0.01
Resolution (temperature)	(°C)	0.1°C
Correctness (pH)		± 0.02
Correctness (at 25°C)	(°C)	± 0.5
Temperature compensation	(°C)	automatic, 0 - 70
Calibration		automatic, 1-2 ponints
Ambient temperature /relative moisture ratio	(°C/%)	0 - 50°C/ max. %95

Figure 4.10. pH meter (Milwaukee MW102)

(Source: Blabmarket.com)

4.4.2 Color Analysis

Color is known as an essential quality criterion in dried tomatoes. Dried tomatoes, which are not attractive in terms of color, are not preferred by the consumer, even if their nutritive properties are the same (Source: Ergün, 2020). Color analysis is carried out to observe the color changes of dried tomatoes due to drying conditions. Konica Minolta CR-400 Color Measurement Device (Chromameter) is used for this analysis (Figure 4.11).

Figure 4.11. Colorimeter (Konica Minolta CR-400)

(Source: Konicaminolta.eu)

The features of the device are given in Table 4.5.

Table 4.5. Konica Minolta CR-400 technical specifications
(Source: Konicaminolta.eu/tr)

Model		**Konica Minolta CR-400**
Lighting/imaging system		d:0° (wide illumination /0° viewing angle; including reflective element)
Detector		Silicon photocell
Display range		Y: %0.01 and %160.00 (reflection)
Source of light		Vibrating xenon bulb
Measuring time	(s)	1
Minimum measuring range	(s)	3
Measuring area /illumination area	(mm)	Ø 8/ Ø 11
Color ranges / colorimetric data		XYZ, Yxy, L*a*b*, Hunter Lab, L*C*h, Munsell ((Illuminator C only), CMC (l:c), CIE1994, Lab99, LCh99, CIE2000, CIE WI/Tw (Illuminator D65 only), WI ASTM E313 (Illuminator C only), YI ASTM D1925 (Illuminator C only), YI ASTM E313 (Illuminant C only)
Ambient temperature / relative moisture ratio	(°C/%)	0-40 °C / %85

The illuminance value L*; ranges from “0” black to “100” white. “a*” value, “-a*” with green, “+a*” with redness; “b*” value indicates blue with “-b*” and yellowness with “+b*”. In addition to these measurements, C* (color intensity) and Hue* angle (color vividness) values are calculated according to Equations 4.14 and 4.15, respectively (Source: Oluk et al., 2012).

$$C^* = [a^2 + b^2]^{1/2} \quad (-) \tag{4.14}$$

$$Hue^* = \frac{180}{\pi} \cos\left(\frac{a}{C^*}\right) \quad (°) \tag{4.15}$$

The higher the C* value, the brighter the color while the lower the value, the more matte the color. The hue value shows the hue angle in degrees, 0° corresponds to the +a axis (red), 90° to the +b axis (yellow), 180° to the –a axis (green), and 270° to the

–b axis (blue) (Source: Oluk et al., 2012). The color diagram used to evaluate these values is shown in Figure 4.12.

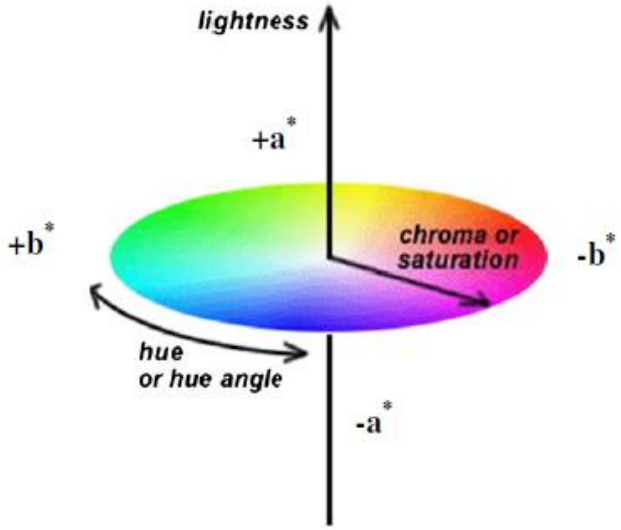

Figure 4.12. Color diagram used to evaluate L*, a* and b* values
(Source: Senkeser, 2018)

4.4.3 Moisture Content Determination

Moisture content; affect the processability, shelf life, usability, and quality of a product. Therefore, the correct determination of moisture plays a fundamental role in ensuring quality in many industries, including food, pharmaceuticals, and chemicals. The moisture in foods is generally determined by drying them in an oven. The evaporation of the water in the sample under a specific temperature and the determination of the moisture content from the weight loss is called moisture determination.

A Memmert UNB 400 oven is used to analyze the moisture content of dried tomato samples (Figure 4.13). The maximum temperature of this oven is 105°C, and it has natural air circulation, an integrated digital timer and LED display visual panel.
Within the scope of the project, the individual weights of the dried tomato slices are taken and placed in the oven preheated to 105°C. The tomato slices are weighed every hour until their masses are constant and dried until the moisture contained in them is completely removed. The moisture content of the dry product is calculated using the weight variation.

Figure 4.13. Oven (Memmert UNB 400)

(Source: Labrehberi.com)

4.5 Energy and Exergy Analysis

Determining the energy and efficiency during the drying process has an essential share in the cost of the dry product. Exergy analysis, on the other hand, contributes to increasing the system's efficiency by determining and improving the losses in the equipment that make up the dryer. For the energy and exergy analysis calculations of the dryer; Tray inlet temperature, tray outlet temperature, ambient temperature, relative humidity and velocity values are used. The flow diagram of energy and exergy analysis is given in Figure 4.14.

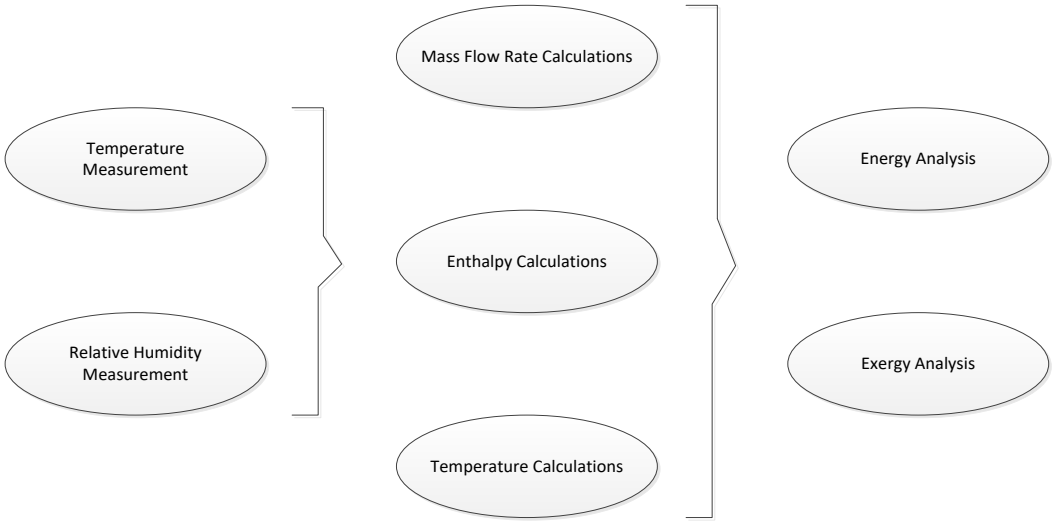

Figure 4.14. Energy and exergy analysis method

4.5.1 Energy Analysis

The dryer is divided into 3 main sections (fan, heat exchanger, drying chamber) for energy analysis, as shown in Figure 4.15. Mass and energy balance equations for each section are given in Equations 4.16-4.32 (Source: Erdem et al., 2021).

HOBO U12-013 measuring devices are used to measure air temperature and relative humidity from the determined points, such as the inlet of the tray, outlet of the tray, and ambient. The technical specifications of the HOBO device are given in Table 4.6.

Table 4.6. HOBO U12-013 technical specifications
(Source: Environmental-expert.com)

Measurement range	Temperature: -20° to 70°C
	RH: 5% to 95% RH
Battery life	1 year typical use
Memory	64K bytes (43,000 12-bit measurements)
Weight	46 g (1.6 oz)
Dimensions	58 x 74 x 22 mm

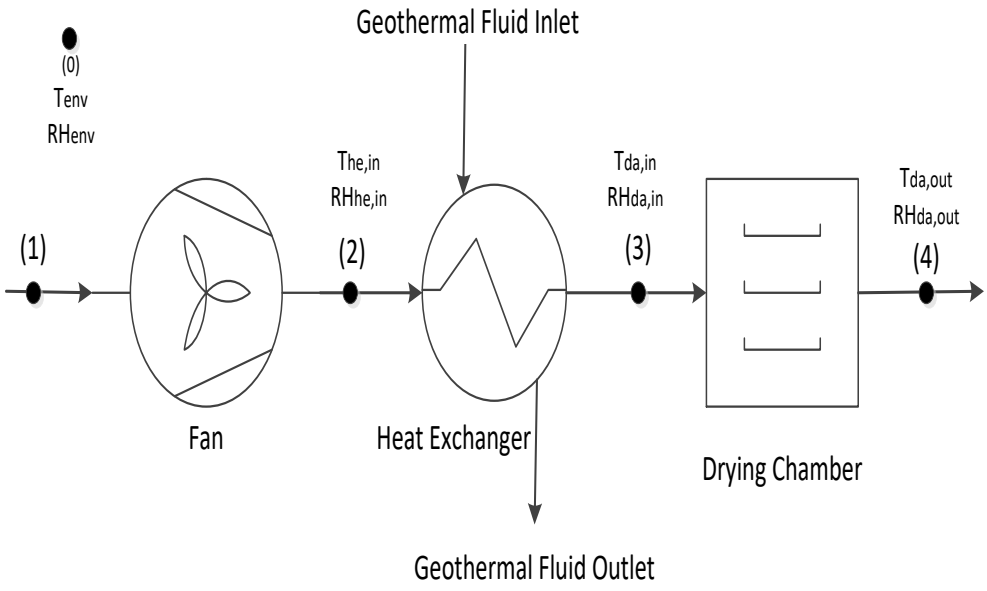

Figure 4.15. Schematic representation of the drying system

$$\dot{m}_{da,env} = \dot{m}_{air,(1)} \quad (kg/s) \tag{4.16}$$

$$\dot{m}_{da,env} * h_{da,env} = \dot{m}_{air,(1)} * h_{air,(1)} \quad (kW) \tag{4.17}$$

Fan:

$$\dot{m}_{air,(1)} = \dot{m}_{air,(2)} = \dot{m}_{da} \quad (kg/s) \tag{4.18}$$

$$Q - W = \sum(\dot{m}_{da})_{in}\left(h_{out} + \frac{V_{out}^2}{2}\right) - \sum(\dot{m}_{da})_{out}\left(h_{out} + \frac{V_{in}^2}{2}\right) \tag{4.19}$$

$$W_{fan} = \dot{m}_{air} * \left(h_2 - h_1 + \frac{v_{da}^2}{2}\right) \quad (kW) \tag{4.20}$$

Heat Exchanger:

For geothermal fluid line:

$$\dot{m}_{water,inlet} = \dot{m}_{water,outlet} \quad (kg/s) \tag{4.21}$$

$$\dot{Q}_{water,inlet} = \dot{m}_{water} * \left(h_{water,inlet} - h_{water,outlet}\right) \quad (kW) \tag{4.22}$$

For drying air:

$$\dot{m}_{air,(2)} = \dot{m}_{air,(3)} = \dot{m}_{da} \quad (kg/s) \tag{4.23}$$

$$\dot{Q}_{air} = \dot{m}_{da} * (h_3 - h_2) \quad (kW) \tag{4.24}$$

Drying Chamber:

$$\sum \dot{m}_{da,(3)} = \sum \dot{m}_{da,(4)} = \dot{m}_{da} \quad (kg/s) \tag{4.25}$$

$$\sum(\dot{m}_w)_{in} + (\dot{m}_w)_{product} = \sum(\dot{m}_w)_{out} \quad (kg/s) \tag{4.26}$$

or

$$\sum(\omega_{da})_{in} * \dot{m}_{da,(3)} + (\dot{m}_w)_{product} = \sum(\omega_{da})_{out} * \dot{m}_{da,(4)} \quad (kg/s) \tag{4.27}$$

Equation 4.28 is used to convert the relative MR of the air at the inlet and outlet of the drying chamber to the MR.

$$\omega = \frac{\emptyset P_{sat@T}}{P - P_{sat@T}} \qquad (kg/kg) \qquad (4.28)$$

The total mass air flowrate required for the drying process is calculated by Equation 4.29.

$$\dot{m}_{da} = \rho_{da} * V_{da} * A_{cr} \qquad (kg/s) \qquad (4.29)$$

The amount of energy (EU) used during the removal of moisture from the product is calculated using Equation 4.30.

$$EU = \dot{m}_{da}\left(h_{da,(3)} - h_{da,(4)}\right) \qquad (kW) \qquad (4.30)$$

The energy utilization rate (EUR) is the ratio of EU to the amount of energy gained by the drying air in the heat exchanger (Equation 4.31).

$$EUR = \frac{\dot{m}_{da}\left(h_{da,(3)} - h_{da,(4)}\right)}{\dot{m}_{da}(h_3 - h_2)} * 100 \qquad (\%) \qquad (4.31)$$

Specific moisture extraction rate (SMER) describes the effectiveness of the energy used in the drying process. SMER is defined as kilogram of moisture removed per kilowatt-hour consumed energy and is related to the total power to the dryer including the fan power and the efficiencies of the electrical devices (Source: Baysal et al., 2015). SMER is described by the following Equation 4.32:

$$SMER = \left(\frac{\text{Amount of water removed during drying}}{\text{Total energy supplied in drying process}}\right) \qquad \left(\frac{kg}{kWh}\right) \qquad (4.32)$$

4.5.2 Exergy Analysis

In any case, the specific exergy is calculated according to Equation 4.33. The total exergy transferred is calculated by multiplying the specific exergy with the flow rate (Equation 4.34) (Source: Filiz et al., 2019).

$$\Psi = (h - h_0) - T_0(s - s_0) \qquad (kJ/kg) \qquad (4.33)$$

$$\dot{E}x = \dot{m}\Psi \qquad (kW) \qquad (4.34)$$

The total exergy equation for ideal gases is given in Equation 4.35.

$$\dot{E}x = \dot{m}_{da}\left(c_p\right)_{da}\left[(T - T_0) - T_0 \ln\frac{T}{T_0}\right] \quad (kW) \qquad (4.35)$$

The exergy balances, exergy losses and exergetic efficiency equations for each component are given in Equation 4.36-4.43.

Fan:

$$\dot{E}x_{dest,fan} = \dot{W}_{fan} + \dot{m}_{da}(\Psi_2 - \Psi_1) \quad (kW) \qquad (4.36)$$

$$\varepsilon_{fan} = \frac{\dot{m}_{da}(\Psi_2 - \Psi_1)}{\dot{W}_{fan}} \qquad (\%) \qquad (4.37)$$

Heat Exchanger:

For geothermal fluid line:

$$\dot{E}x_{dest,water} = \dot{m}_{water}(\Psi_{water,in} - \Psi_{water,out}) \quad (kW) \qquad (4.38)$$

For drying air:

$$\dot{E}x_{dest,air} = \dot{m}_{da}(\Psi_3 - \Psi_2) \qquad (kW) \qquad (4.39)$$

$$\varepsilon_{he} = \frac{\dot{m}_{da}(\Psi_3 - \Psi_2)}{\dot{m}_{water}(\Psi_{water,in} - \Psi_{water,out})} \qquad (\%) \qquad (4.40)$$

Drying Chamber:

$$\dot{E}x_{dest,dc} = \dot{m}_{da}(\Psi_3 - \Psi_4) \qquad (kW) \qquad (4.41)$$

$$\varepsilon_{dc} = \frac{(\text{Inlet flow energy} - \text{Outlet flow energy})}{\text{Inlet flow exergy}} \qquad (\%) \qquad (4.42)$$

or

$$\varepsilon_{dc} = 1 - \frac{\dot{m}_{da}(\Psi_3 - \Psi_4)}{\dot{m}_{da}\Psi_3} \qquad (\%) \qquad (4.43)$$

Assumptions are made for exergy analysis are:

1. Drying process takes place under equilibrium conditions (independent of time) and constant flow conditions.

2. Potential and kinetic energy changes are neglected.

3. The drying air is ideal gas, its specific heat is assumed to have throughout the whole process.

4. The dead state temperature (To) was taken as the ambient temperature (Tenv) measured in each experiment.

5. Dead state pressure Po is atmospheric pressure.

4.6 Experiment Design

Two factor, face centred central composite design is applied and response surface methodology is used to determine the main and interaction effects of drying air temperature and velocity on quality parameters of dried tomato slices. Statistical models with interaction terms are derived to examine the relative significance of the two variables, drying air temperature (X_1) and drying air velocity (X_2) and their interactions on the responses, pH value (Y_1), color value (Y_2) and moisture ratio value (Y_3). The independent variables, their values, and levels, as products of the dependent variables, are shown in Table 4.7.

Table 4.7. Central composite design variables

Independent variables (coded)	-1	0	1
X_1 = Temperature (°C)	40	60	80
X_2 = Air velocity (m/s)	0,5	-	1,5
Dependent variables	Y_1 = pH value		
	Y_2 = Color value		
	Y_3 = Moisture ratio value		

The central composite design matrix is shown in Table 4.8. Each line shows an experiment with coded levels.

Table 4.8. Central composite design matrix

Experiment number	Temperature (°C)	Air velocity (m/s)
1	(0)	(1)
2	(1)	(1)
3	(-1)	(1)
4	(0)	(-1)
5	(1)	(-1)
6	(-1)	(-1)

4.7 CFD Modelling

CFD provides a qualitative prediction of fluid flows based on the conservation laws (conservation of mass, momentum, and energy) governing fluid motion, by means of mathematical modeling (partial differential equations), numerical methods (discretization and solution techniques) and software tools (solvers, pre- and postprocessing utilities). CFD gives an insight into flow patterns that are difficult, expensive or impossible. As a rule, CFD does not replace the measurements completely but the amount of experimentation and the overall cost can be significantly reduced (Source: Kuzmin, 2004).

4.7.1 Governing Model Equations

A simplified schematic diagram of the drier cabinet is given in Figure 4.16. Once slice of tomato is located at the base of the cabinet.

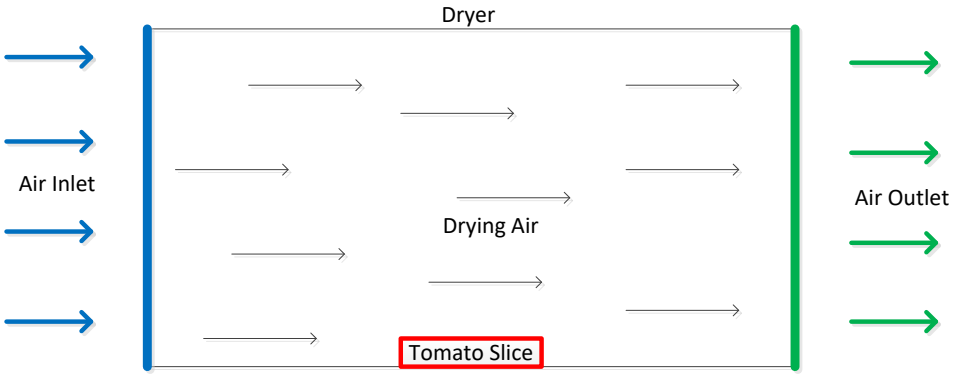

Figure 4.16. Simulation of the dryer

The following assumptions are made during the analysis;

- Fluid is Newtonian
- Flow is steady
- Flow is incompressible
- Work effect is neglected
- All features are fixed
- No viscous dispersion
- $\mathrm{Re} = \frac{\rho V L}{\mu} \rightarrow 19166.6 \text{ for } 0.5 \text{ m/s and } 57499.9 \text{ for } 1.5 \text{ m/s}$

Both of them are lower than $5 * 10^5$. Therefore, the flow is accepted as LAMINAR.

The mass, momentum and energy balance equations are formulated together to simulate the velocity, air temperature, tomato slice moisture and tomato slice temperature distribution in the tray dryer.

Momentum Equations

Based on conservation of momentum, the governing equation for air transport towards the product is given in Equation 4.45.

$$\rho \frac{\partial u}{\partial t} + \rho(u.\nabla)u = \nabla.[-\rho I + \mu(\nabla u + (\nabla u)^T)] \quad (4.45)$$

$$\frac{\partial \rho}{\partial t} + \nabla.u = 0 \quad (4.46)$$

The flow through the sample domain (for our experiment, tomato slice) is considered zero, $\frac{\partial \rho}{\partial t} = 0$ and the final equation is given by Equation 4.46 for fluid domain and Equation 4.47 for no-slip boundary equations. A fluid domain is used to define a region of the computational domain occupied by vacuum or by a fluid specified by its material properties. In fluid dynamics, the no-slip boundary condition for viscous fluids assumes that at a solid boundary, the fluid will have zero velocity (Equation 4.48) relative to the boundary (Source: Day, 2004).

$$\rho(u.\nabla)u = \nabla.[-\rho I + \mu(\nabla u + (\nabla u)^T)] \quad (4.47)$$

$$\nabla.u = 0 \quad (4.48)$$

Mass Transfer Equations

The conservation of mass equation for water transport in the product sample is given by Equation 4.49 (Source: Belay, 2020).

$$\frac{\partial c}{\partial t} + \nabla(-D\nabla c) + u_i \nabla c = R \tag{4.49}$$

In Equation 4.49, the first component indicates moisture accumulation within tomato slices, the second component indicates moisture transport within tomato slices due to diffusion, and the third component indicates convection due to fluid flow. The term (R) on the right is the mass flow evaporating from the porous medium (tomato slices).

The phase change between liquid water and vapor (evaporation), M_{evap}, is defined by the Equation 4.50.

$$M_{evap} = K_{evap}\left(a_w c_{v,sat} - c_v\right) \tag{4.50}$$

$$a_w = \exp\left(-0.0267 X_{db}^{-1.656} + 0.0107 X_{db}^{1.151} \exp(-1.287 X_{db})\right) \tag{4.51}$$

Where K_{evap} is an evaporative constant, a_w water activity which is a function of dry bass moisture content (X_{db}).

The value of moisture concentration (c) in Equation 4.49 is designated by C_l for liquid phase Equation 4.52 and C_v for vapor phase Equation 4.53.

$$C_l = \rho_w \varepsilon S_w \tag{4.52}$$

$$C_v = p_v M_w \varepsilon S_g \tag{4.53}$$

Heat Transfer Equations

The equations for heat transfer at the solid interface for the temperature (T) calculation in tomato slices are given in Equation 4.54.

$$\rho_{eff} c_{p,eff} \frac{\partial T}{\partial t} = \nabla(\lambda_{eff} \nabla T) + Q \tag{4.54}$$

Energy, required for evaporation, is calculated by Equation 4.55.

$$Q = -\dot{m_{LG}} \Delta H_{vap} \quad (kW) \tag{4.55}$$

Where ΔH is the latent heat of vaporization (J/kg). In this case, the effective density ρ_{eff} and effective heat capacity $c_{p,eff}$ are calculated with the help of Equation 4.56 and Equation 4.57.

$$\rho_{eff} = \theta_L\rho_L + \theta_S\rho_S + \theta_G\rho_G \quad (kg/m^3) \qquad (4.56)$$

$$c_{p,eff} = \left(\theta_L\rho_L c_{p,L} + \theta_S\rho_S c_{p,S} + \theta_G\rho_G c_{p,G}\right)/\rho_{eff} \qquad (4.57)$$

where θ_L, θ_S, and θ_G represent the volume fraction of the liquid, solid, and gas phases in the tomato slices, respectively. The effective thermal conductivity is calculated with Equation 4.58.

$$\lambda_{eff} = \lambda_{dry} + \frac{\theta_L}{1-\theta_S}\left(\lambda_{wet} - \lambda_{dry}\right) \quad (W/m.K) \qquad (4.58)$$

Where λ_{dry} and λ_{wet} are the thermal conductivities of the dry and fully saturated tomato slices, respectively.

Inside the tomato slices, the overall liquid and gaseous phases contribute to the heat convection term. Averaged thermal properties are required, density (ρ), heat capacity (c_p), and thermal conductivity (λ) are calculated using Equations 4.59-4.61.

$$\rho_{tot} = S_G\rho_{ma} + S_L\rho_w \qquad (kg/m^3) \qquad (4.59)$$

$$c_{p,tot} = \frac{S_G\rho_{ma}c_{p,ma} + S_L\rho_w c_{p,w}}{\rho_{tot}} \qquad (J/kg.K) \qquad (4.60)$$

$$\lambda_{tot} = S_G\lambda_{ma} + S_L\lambda_w \qquad (W/m.K) \qquad (4.61)$$

In these equations, S represents the saturation variables, m_a represents moist air and w represents water.

Finally, the heat of evaporation can be calculated with the help of Equation 4.62:

$$Q = -H_{vap}m_{vap} \qquad (kW) \qquad (4.62)$$

where H_{vap} (J/mol) is the latent heat of evaporation.

The steady-state airflow process at T=40-60-80°C, v=0.5-1.5 m/s in a rectangular duct (Fig. 4.16) is considered for CFD modelling. The drying process with a single tomato slice at the base is modelled. As a result of the experimental and simulation moisture content values, the error rate is calculated with the help of Equation

4.63. An error of up to 10% is the expected range, but up to 25% is acceptable (Source: Frost, 2017; Belay, 2020).

$$\text{Error } \% = \frac{|(\text{Experimental MC} - \text{Simulation MC})|}{\text{Simulation MC}} * 100 \qquad (4.63)$$

The material dried during the design is tomato, and the material that circulates in the dryer is air. Technical data for the materials used are listed in Table 4.10.

Table 4.9. Boundary conditions

Flow	**v (m/s)**	**P (atm)**	**T (°C)**
Inflow	0.5-1.5	1	40-60-80
Outflow	?	1	$\frac{\partial T}{\partial x} = 0$

Table 4.10. Technical data of the materials used

Material	**Thermal conductivity (W/m.K)**	**Density (kg/m^3)**	**Heat capacity (J/kg.K)**
Drying air	0.025	1.127	1006
Tomato slices	0.628	470	3977.46

4.7.2 Geometrical Model Setup and Mesh Generation

The geothermal cabinet dryer geometric setup is shown in Figure 4.17a. The drying chamber is 0.65 m in width and 0.25 m in height for 2D geometrical modeling. There are no trays while modeling the drying process. Tomato slice is considered as porous media spread 7 mm thick on the base. In the meshing section, the computational space is divided into smaller control volumes using the mesh section in the COMSOL Multiphysics software (Fig. 4.17b). During the mesh of this modeling, 33630 triangles and 8112 quads; a total of 41742 elements are used.

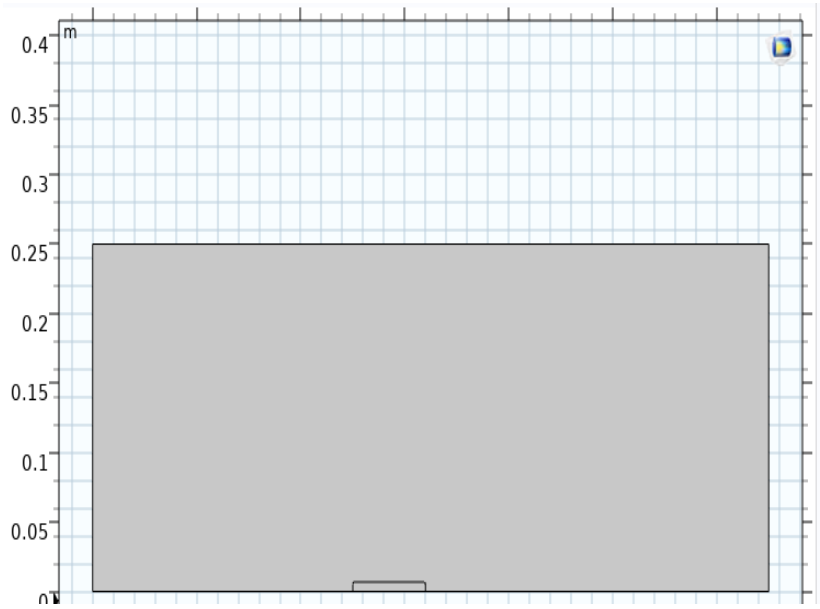

(a)

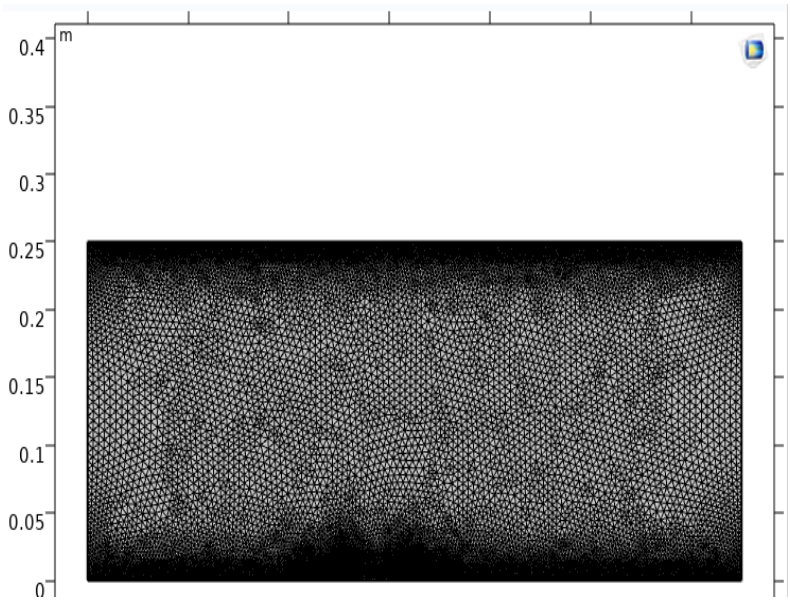

(b)

Figure 4.17. Geothermal cabinet dryer (a) geometrical and (b) mesh setup

A grid independence test is performed to ensure the accuracy of the numerical results. It is also essential to ensure the appropriate grid cell size to obtain accurate simulation results. Table 4.11 and Figure 4.18 compare the number of grids and the temperature values. It is seen that the temperature value converges as the number of grid cells increases.

Table 4.11. Grid independency test results

Temperature (°C)	Number of mesh
26.01394	1333
25.02171	2098
24.23274	3233
23.82922	4861
23.48776	8678
23.49329	11816
23.62328	17393
23.63932	24955
23.81864	41742
23.83487	70076
23.82585	164608

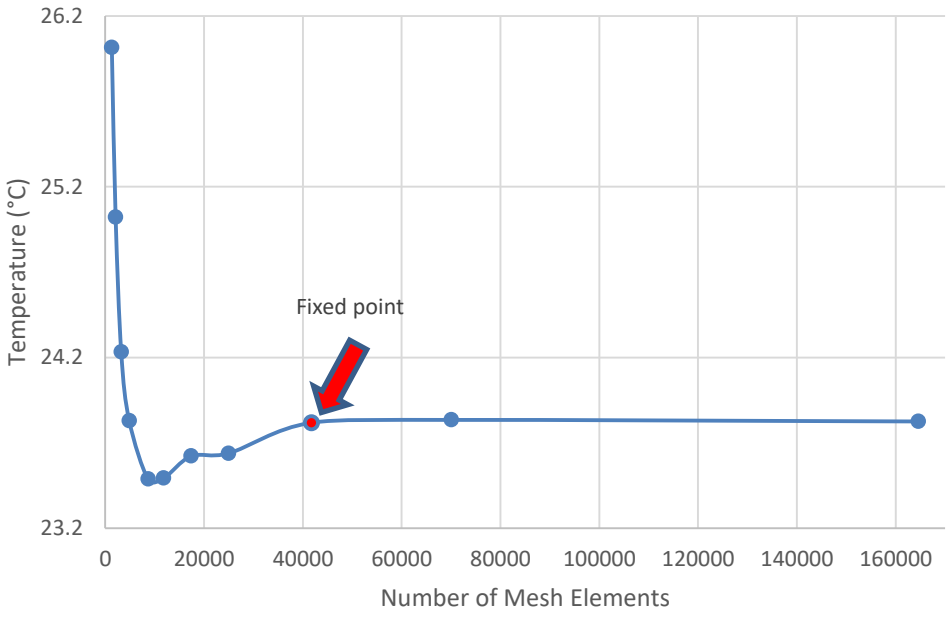

Figure 4.18. Grid independency test results

CHAPTER 5

RESULTS AND DISCUSSION

This Thesis consists of two main parts as experimental and CFD modeling. In the experimental part, the effects of drying air temperature and velocity on the drying process and product quality are evaluated. In the modeling part, the drying process is modelled by Comsol Multiphysics software. Then, model is simulated for various drying air conditions and the simulation results are compared with experimental results. Also, results are validated by experimental data.

5.1 Drying Experiments

To determine the effect of drying air and temperature on tomato drying kinetics, tomatoes are collected and dried in a geothermal dryer with different drying air temperature (40-60-80°C) and velocity (0.5-1.5 m/s) combinations. Depending on the drying time, MR values are determined for each experiment. In order to evaluate the quality parameters of fresh and dried tomatoes; pH, color, and moisture content measurements are conducted. Furthermore, thin layer models that are suitable for the experimental results are determined by statistical analysis. In order to determine the performance of the drying system, energy and exergy analyses are performed. In total, six experiments are carried out. The drying air temperature and velocity values of the experiments are given in the table.

Table 5.1. Experimental conditions

Experiment no.	**1**	**2**	**3**	**4**	**5**	**6**
Temperature (°C)	40	40	60	60	80	80
Air velocity (m/s)	0.5	1.5	0.5	1.5	0.5	1.5

5.1.1 Determination of Initial Moisture Content

Prior to the experiments, tomato slices are desiccant-dried at high temperatures for about 6 hours to determine the initial moisture content. An analytical balance with an accuracy of ± 0.001 g is used to weigh the samples (Figure 5.1a). Pre- and post-

drying appearances of tomato slices are given in Figures 5.1b and 5.1c. The initial moisture content of tomatoes is determined as 93.8%. The moisture content of dried tomatoes is expected to be 1-10% (Source: Sahin, 2010; Ozen, 2018). In the Thesis, the final moisture content is intended to be 8%. Thus, the amount of moisture to be removed during the experiments is 85.8%. Two trays are actively used during the experiments. Considering that there are 150 slices of tomatoes in each tray, there will be an average of 300 tomato slices in two trays. Since six experiments carry out in total, approximately 1800 slices of tomatoes dry. An average of 6 slices are obtained from each tomato. As a result, 300 tomatoes are used during all drying processes.

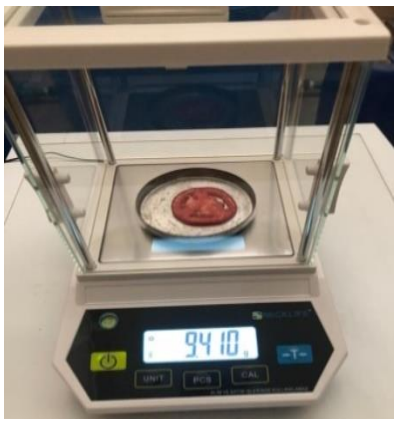

(a)

(b)

(c)

Figure 5.1. (a) Weighing of tomato slices, (b) appearance of tomato slices before moisture determination, (c) appearance of tomato slices after moisture determination

5.1.2 Drying Characteristics

In this section, the results obtained from the experiments are presented. Drying time, MR, and drying velocity; are investigated under specified temperatures (40-60-80°C) and velocities (0.5-1.5 m/s).

5.1.2.1 Effect of Drying Air Temperature

Drying time

Drying time is the duration that initial moisture content is reduced to 0-10%. Table 5.2 and Figure 5.2 give the drying time for each experiment.

Table 5.2. Drying time depending on air temperature at constant air velocities

Air velocity (m/s)	Temperature (°C)	Drying time (min)
0.5	40	360
	60	255
	80	180
1.5	40	240
	60	180
	80	115

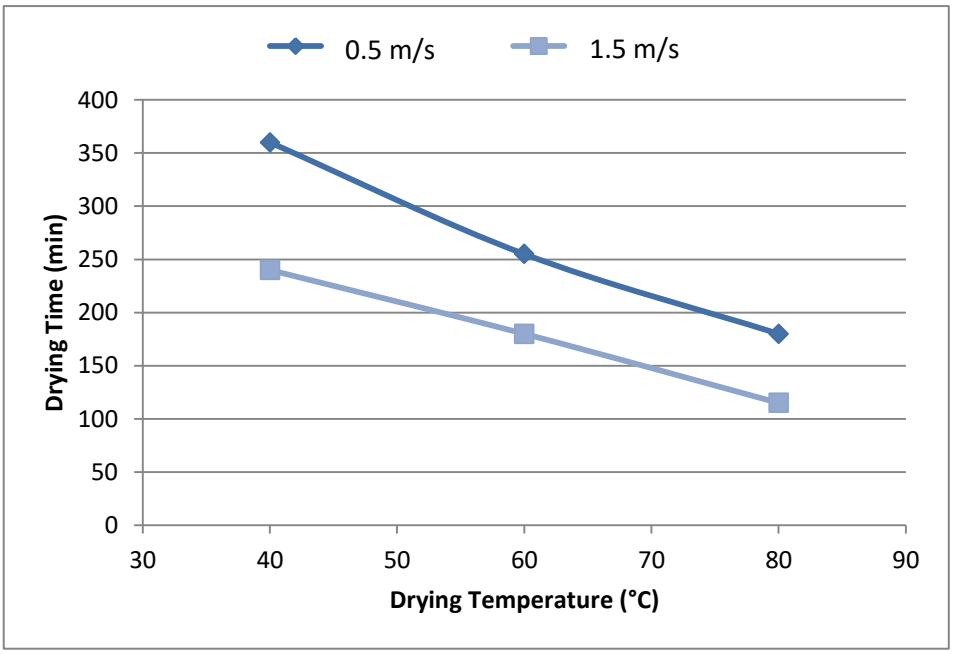

Figure 5.2. Change of drying time with drying air temperature at constant drying air velocities

As can be seen from Table 5.2 and Figure 5.2, increase in drying air temperature at constant air velocity, reduces the drying time. The relationship between temperature and drying time is not linear. The duration of the experiments where the air velocity is 1.5 m/s is shorter than the ones at 0.5 m/s. The longest experiment takes place at a temperature of 40°C and a velocity of 0.5 m/s and lasted for 360 minutes (6 hours). The shortest experiment occurred at 80°C and 1.5 m/s for 115 minutes (1 hour and 55 minutes).

Moisture ratio

MR is a function of drying time. MR-drying time graphs for various drying air temperatures at constant air velocities are shown in Figure 5.3. The Figure indicates that at constant air velocities, drying time decreases with the increased air temperature. If Figure 5.3a (v=0.5 m/s) is compared with Figure 5.3b (v=1.5 m/s), it can be observed that the drying time decreases with the increase in air velocity. In the studies of Stegou-Sagia and Fragkou (2015), the similarity is observed in the graphs of MR versus drying time at temperatures of 50-60-65°C at a constant air velocity while drying mushrooms.

Drying rate

The variation of drying rate with MR at various drying air temperatures for constant drying air velocities is shown in Figure 5.4. With the decrease in the moisture (water) in the product, the diffusion in the product decreases, so the moisture transfer to the product surface becomes difficult. As can be seen in Figure 5.4, a high drying rate is observed at high MR values, while the drying rate decreases as the MR decreases.

It can also be seen from Figure 5.4 that the drying air temperature has a significant effect on moisture removal. When comparing drying rates at 80°C, 60°C, and 40°C, drying rates at 80°C are higher than the other temperatures, which corresponds to lower drying times.. High temperature causes a higher water vapor pressure difference which results in an accelerated water migration through the product. At constant drying air velocity, higher drying air temperature produces a higher drying rate, consequently reducing the drying time. As seen in Figure 5.4, the falling rate drying period is visible in all curves except for the 80°C-1.5 m/s curve. The constant rate drying period is also observed at Figure 5.4.a in a MR range of 0.68 to 0.44 at 40°C, 0.35 to 0.25 at 60°C, and 0.5 to 0.1 at 80°C. Similarly, the constant rate drying period can be observed at Figure 5.4.b in the MR range of 0.9 to 0.69 at 40°C, 0.6 to 0.45 at 60°C, and 0.85 to 0.66 at 80°C.

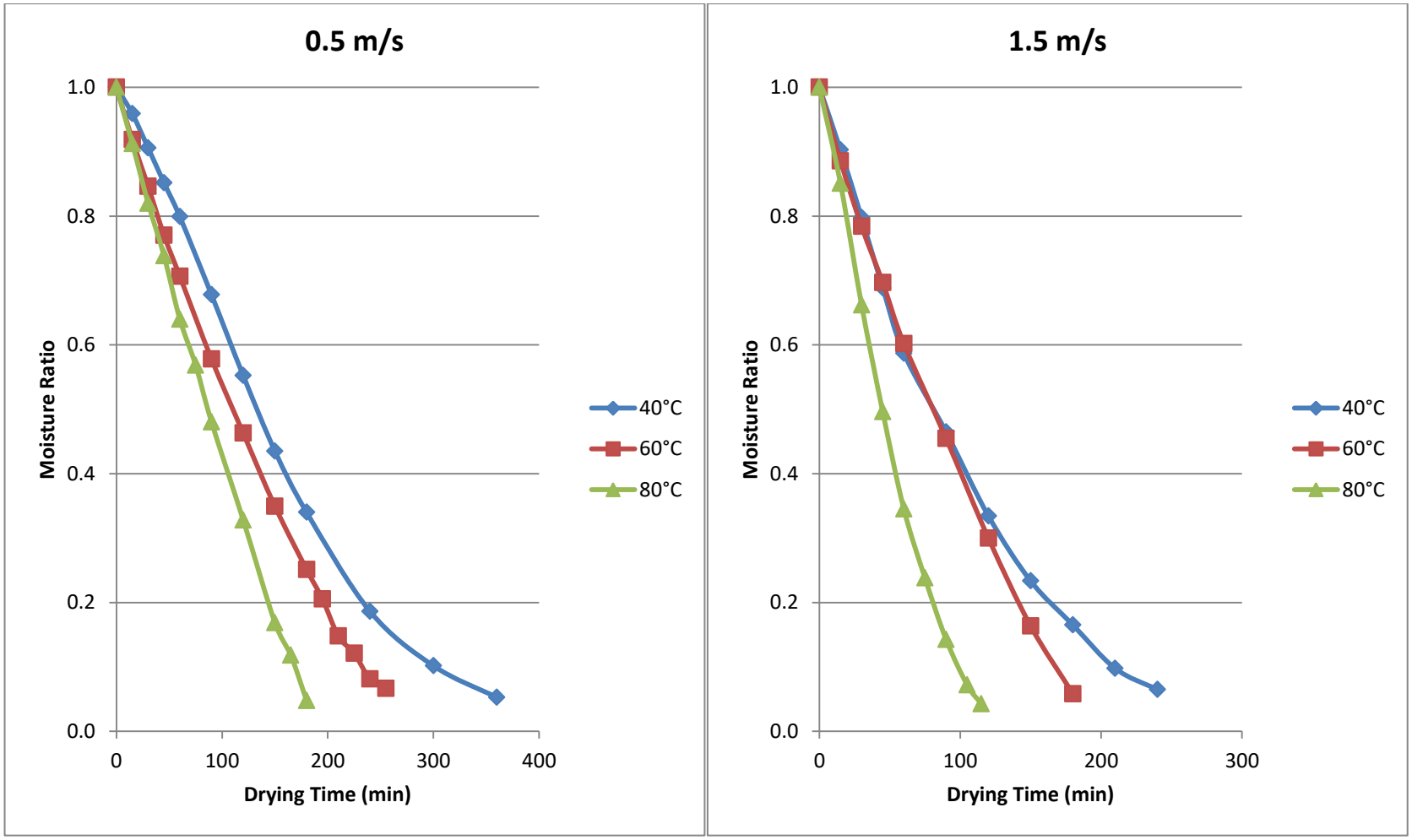

(a) (b)

Figure 5.3. Moisture ratio vs. drying time at various air temperatures for constant velocities (a) v=0.5 m/s, (b) v=1.5 m/s

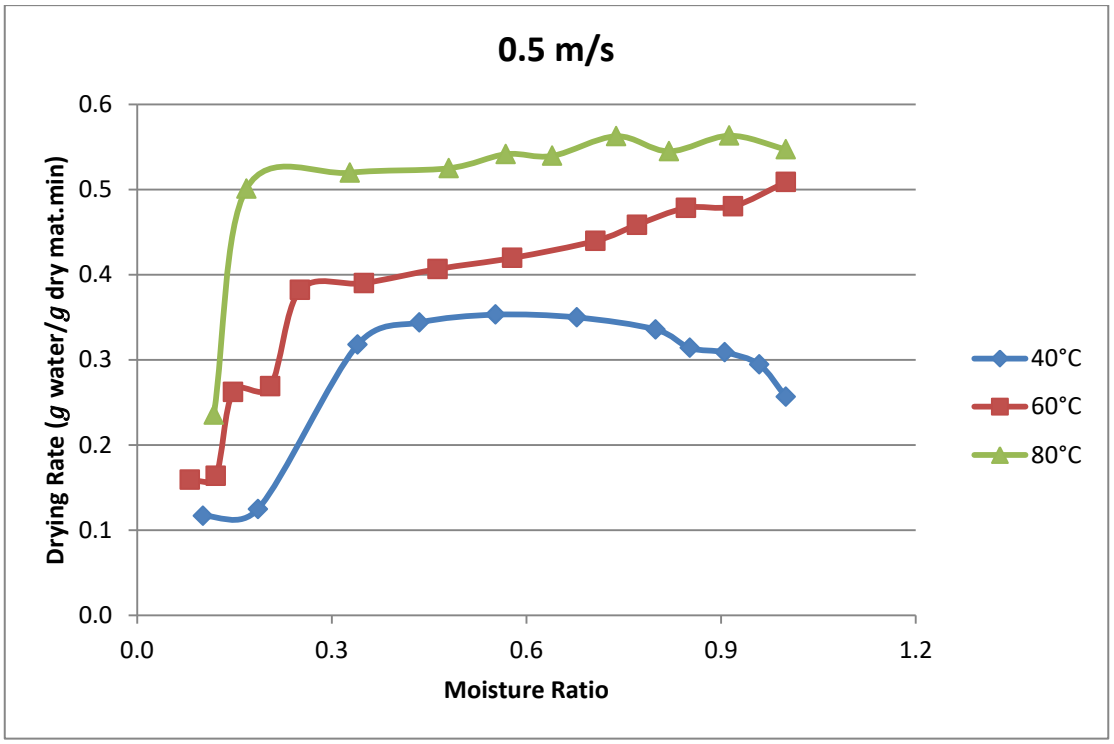

(a)

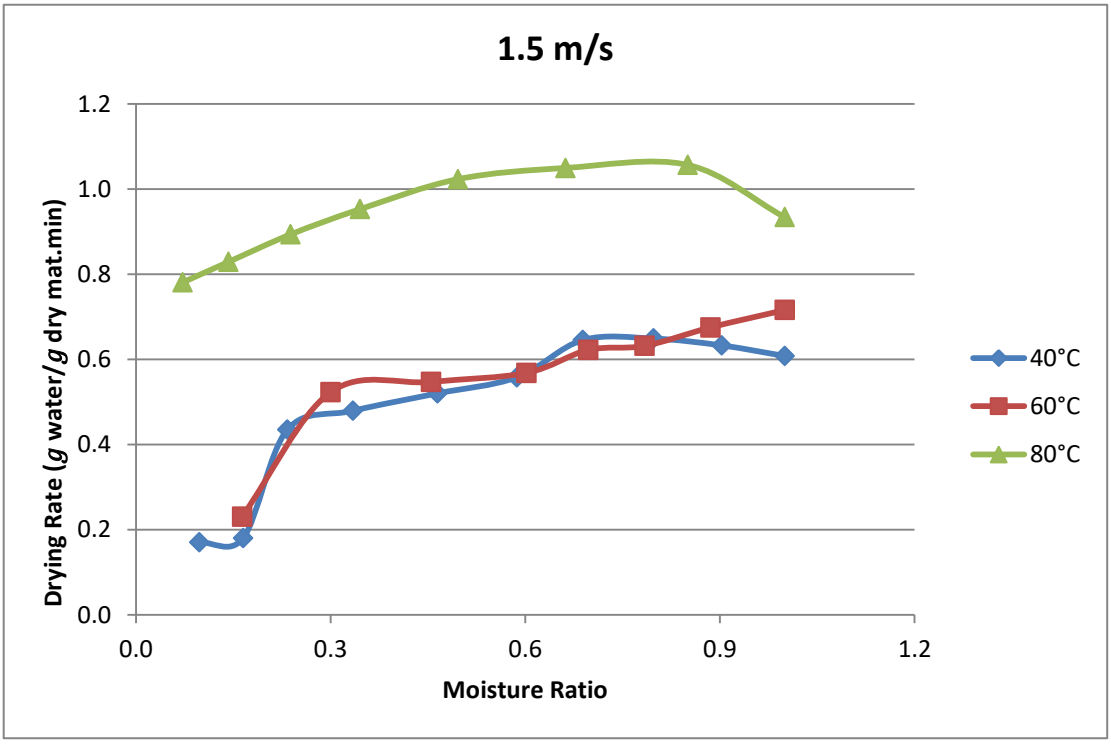

(b)

Figure 5.4. Variation of drying rate and moisture ratio rate with temperature at different air velocities

5.1.2.2 The Effect of Drying Air Velocity

Drying time

Drying time for varying drying air velocities at constant temperatures are given in Table 5.3 and Figure 5.5. As can be seen from the Table and Figure, increasing air velocity causes a decrease in drying time at constant air temperatures. The fastest drying is achieved at 80°C-1.5 m/s, and the slowest drying is achieved at 40°C-0.5 m/s as expected. An increase in air velocity at constant temperature reduces drying time.

Table 5.3. Drying time depends on air velocities at constant air temperatures

Temperature (°C)	Air velocity (m/s)	Drying time (min)
40	0.5	360
	1.5	240
60	0.5	255
	1.5	180
80	0.5	180
	1.5	115

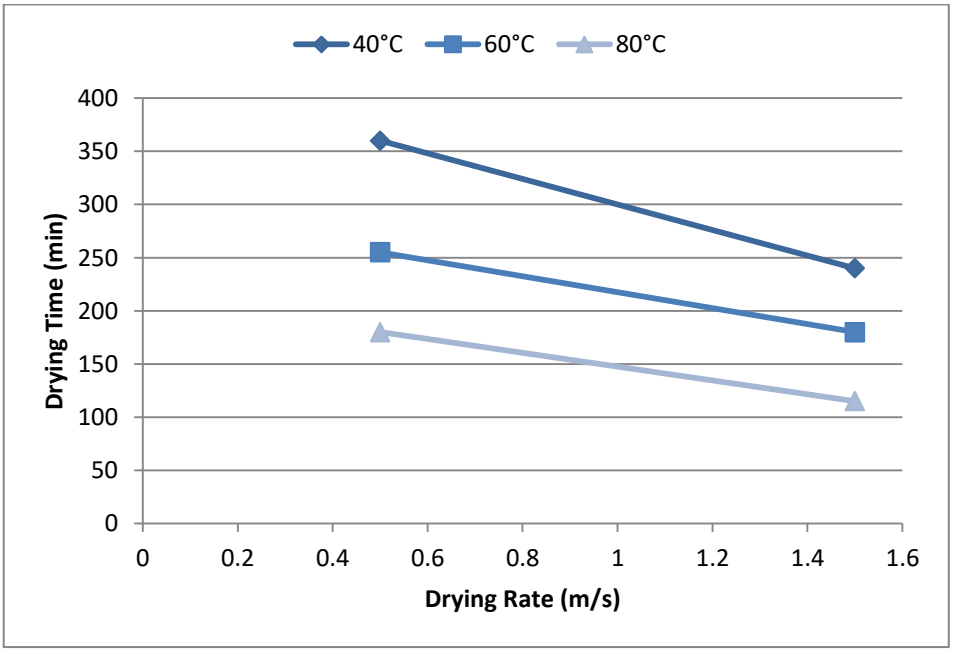

Figure 5.5. The effect of drying air velocity on drying time

Moisture ratio

MR-drying time graphs at constant temperature and different air velocities are shown in Figure 5.6. For constant air temperature, It is observed that the drying time of the products decreased with the increase in air velocity. For constant air velocity, It is observed that the drying time of the products decreased with the increase in temperature. Thus, the targeted MR (0-10%) is reached as a result of the experiment.

In the studies of Stegou – Sagia and Fragkou (2015), the similarity is observed in the graphs of MR versus drying time at 1-2-3-5 m/s air velocities at constant drying temperature drying mushrooms. Aktas et al. (2014) showed similarity in the graphs they obtained from drying the orange peel. Ozgen's (2014) studies observed similarity in the MR versus drying time graphs at 0.5-1-1.5 m/s air velocities at constant drying temperature while drying apples.

Drying rate

The variation of MR and drying rate depending on the drying air velocity at constant air temperatures is shown in Figure 5.7. The drying rate shows a decreasing trend throughout the drying process. In these curves, it is observed that the drying air velocity has a significant effect on moisture removal.

As seen in Figure 5.7, the falling drying period is visible in all curves. In addition, during the continuous drying period in the curves, during the experiment at 40°C-1.5 m/s, the MR decreased from 0.8 to 0.7; In the 40°C-0.5 m/s experiment, in the process where the MR drops from 0.68 to 0.44; In the 60°C-1.5 m/s experiment, in the process where the MR drops from 0.6 to 0.3; During the experiment at 60°C-0.5 m/s, the MR decreased from almost 0.46 to 0.25; In the 80°C-1.5 m/s experiment, in the process where the MR drops from 0.85 to 0.66 and finally, during the experiment at 80°C-0.5 m/s, the MR decreased from almost 1 to 0.57.

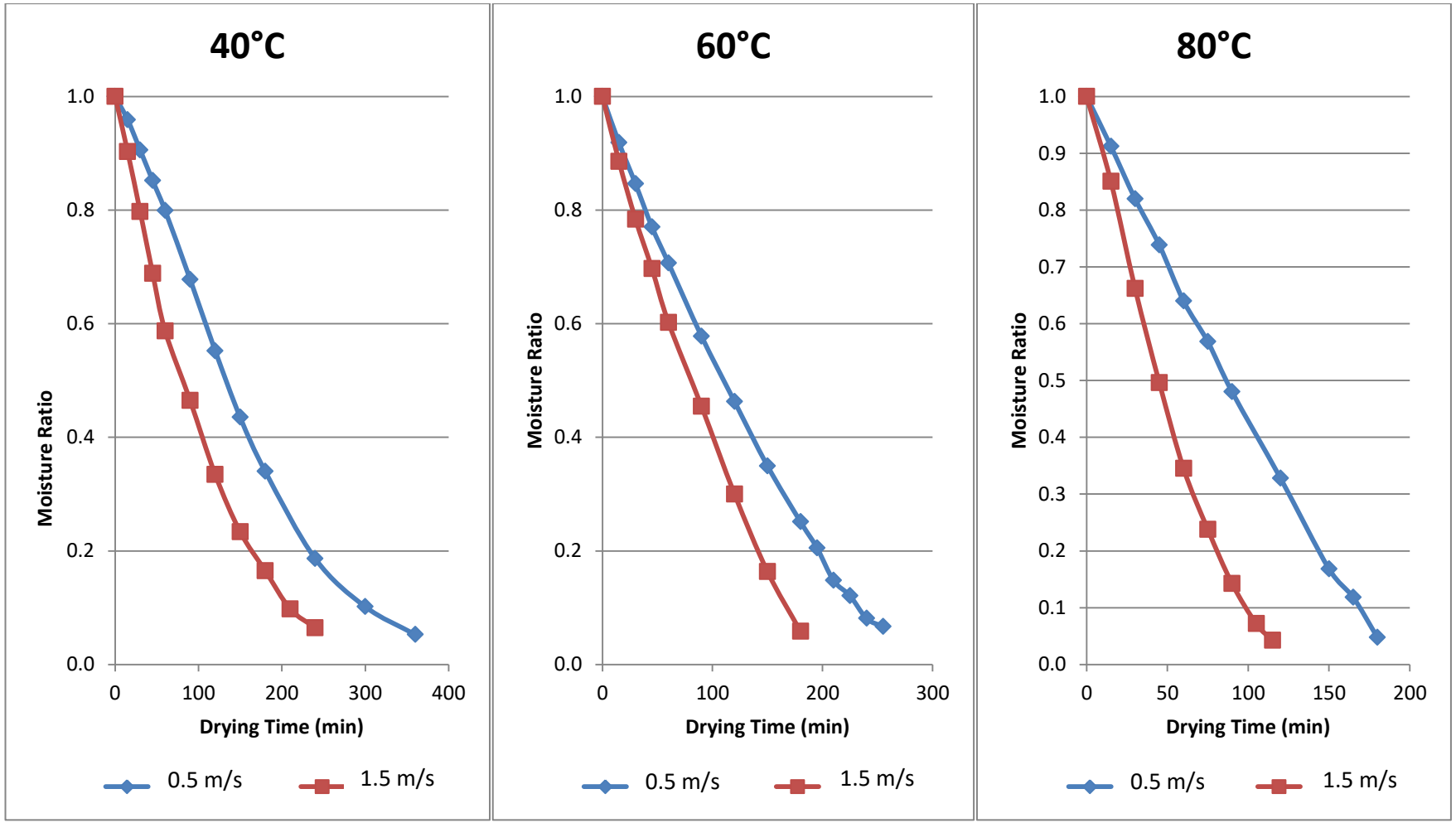

(a) (b) (c)

Figure 5.6. Moisture ratio and drying time (a) at 40°C air temperature, (b) at 60°C air temperature and (c) at 80°C air temperature

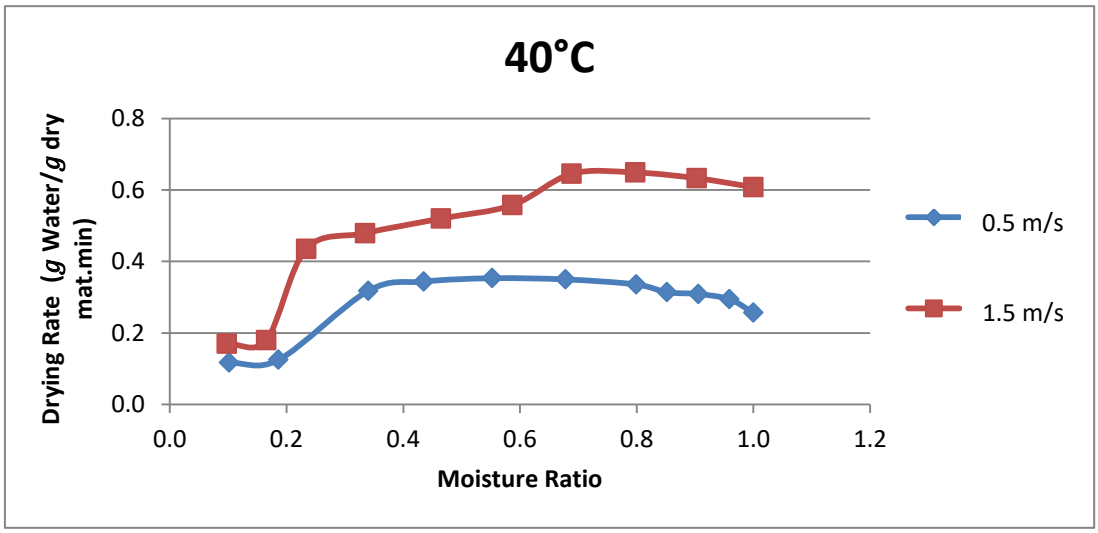

(a)

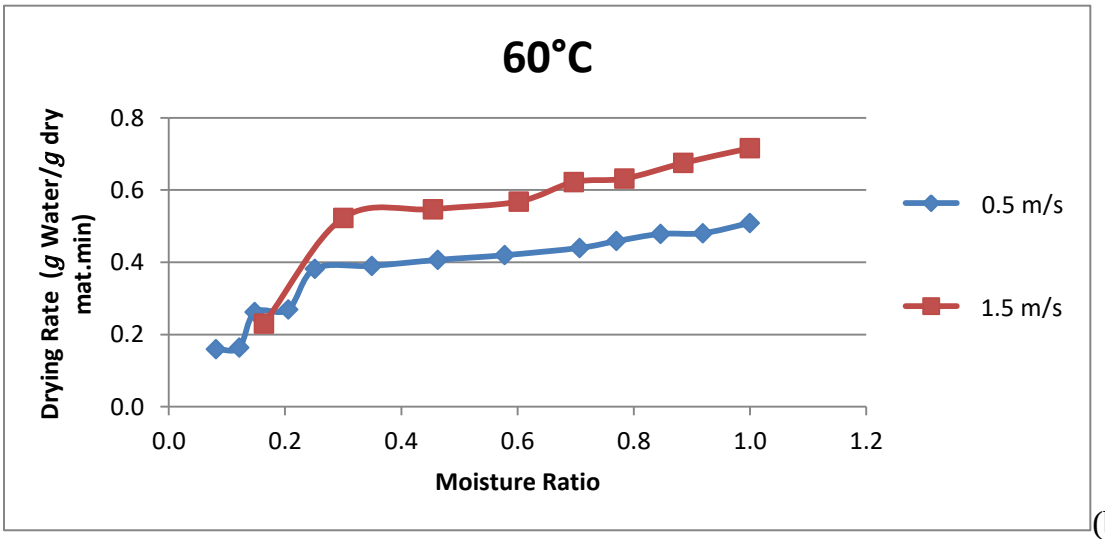

(b)

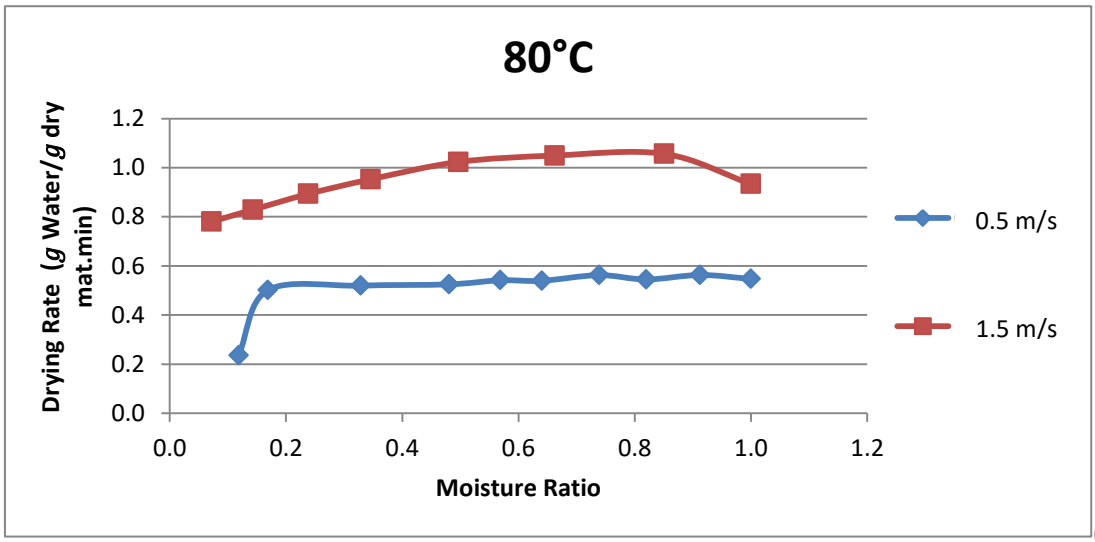

(c)

Figure 5.7. Drying rate and moisture ratio (a) at 40°C, (b) at 60°C and (c) at 80°C air temperature

5.2 Quality Parameters

Quality parameters of dried products are the limiting parameters to determine drying air conditions. Depending on the required pH, color and moisture content of dried tomatoes, drying air temperature and velocity can be specified.

5.2.1 pH Analysis

Tomato is an acidic fruit with a pH value of 4-4.5 (Source: Ergün et al., 2020). These values can be accepted as the same for fresh and dried tomatoes. pH measurements are conducted by a Milwaukee MW102 device before and after the drying process. The measurements are carried out in fresh products by inserting pH meter probes into fresh tomatoes (Figure 5.8) and the result are given in Table 5.4. The pH values of the dried tomatoes are read by fixing the pH meter probes to the fleshy parts of the dried tomatoes. The pH values of dry products under different test conditions are given in Table 5.5.

Figure 5.8. pH measurement of fresh tomatoes

Table 5.4. pH values of fresh tomatoes

pH	
Measurement 1	4.02
Measurement 2	4.12
Measurement 3	4.66
Average	**4.27**

Table 5.5. pH values of dried tomatoes

Experimental condition	80°C 1.5 m/s	80°C 0.5 m/s	60°C 1.5 m/s	60°C 0.5 m/s	40°C 1.5 m/s	40°C 0.5 m/s
pH	4.58	4.16	4.06	4.1	4.86	4.49
Average pH	4.38					

Table 5.4 and 5.5 indicate that the pH values of tomatoes are in the reference range. In addition, it is observed that pH values of dried tomatoes are 2.6-7.8% higher than the fresh tomatoes.

5.2.2 Color Analysis

Color is known as an essential quality criterion in dried tomatoes. Even if their nutritional properties are the same, dried tomatoes that are not attractive in terms of color are not preferred by the consumer (Source: Ergün et al., 2020). Color measurements in terms of L* (brightness), a* (red-green), and b* (yellow-blue) are conducted by using a Minolta colorimeter from the outer surface of dried tomato samples taken from each experiment (Figure 5.9). C*, which gives color intensity, and Hue* angle, which gives color vibrancy, is calculated according to Equation 4.11 and 4.12, respectively. Color analysis results of fresh and dried tomatoes are given in Table 5.6 and 5.7, respectively. Statistical ANOVA analysis is applied to all color values in terms of drying air temperature and velocity, and the p-value obtained as less than 0.05 which means that L*, a*, b*, C*, and hue angle values are insignificant. The Tables show that L* values of fresh tomatoes change between 30.33 and 35.17, while the same values are in the range of 37.58-48.31 for dried ones. This means that the brightness in dried products increases relative to the brightness in fresh products. No significant change is observed in the a* values while the redness value remained approximately the same in fresh and dried tomatoes. In contrast, the b* values increased in dried tomatoes compared to fresh tomatoes, and the yellowness values of the products increased.

In general, it has been determined that the drying temperature increases the product's brightness value. The highest chroma increase in tomatoes occurred at 60°C-0.5 m/s. The parameter in which the chroma value changed the least is the condition of 40°C-1.5 m/s. However, it is determined that the hue angle values increased slightly in all experimental conditions. When the color, one of the essential characteristics of dried tomatoes, is evaluated, the L*, a*, b*, and C* values of the tomatoes in the 40°C-1.5

m/s experiment are lower. This indicates that the color of the fruit is darker and duller than the others. There is no specific reference range for color values. Color values do not affect the consumption characteristics of tomatoes. However, having a dark color can visually make it look bad to the buyer. For this reason, dark-colored dried tomatoes are expected to be less preferred than light-colored ones. It is determined that the L*, a*, b*, and C* values of tomatoes are the highest, which means the best color values (highest brightness and redness), in the 80°C-0.5 m/s experiment.

Ayan (2010) determined that in tomatoes dried at different drying temperatures and drying times, L* values varied between 40.89 and 49.33, a* values between 11.12 and 18.04, and b* values between 8.47 and 12.49. In this study, L* values varied between 37.58 and 48.31, a* values between 27.68 and 33.25, and b* values between 26.99 and 31.74 for dried tomatoes. When the Ayan (2010) and this study are compared; although L* values are approximately the same, a* and b* values are higher in this study. This means that the dried tomatoes in this study had higher rates of redness and yellowness than Ayan (2010)'s study.

Figure 5.9. Dry product samples and color measurement

Table 5.6. Color analysis values of fresh tomatoes

L* (brightness)				**a* (red (+)/green(−))**				**b* (yellow(+)/blue(−))**				**C* (color intensity)**	**Hue* angle**
1	**2**	**3**	**Avg.**	**1**	**2**	**3**	**Avg.**	**1**	**2**	**3**	**Avg.**		
30.33	35.17	33.29	32.93	33.24	31.87	35.72	33.61	20.83	21.41	24.23	22.16	40.26	38.46

Table 5.7. Color analysis values of dried tomatoes

Experimental conditions	**L* (brightness)**	**a* (red(+)/green(−))**	**b* (yellow(+)/blue(−))**	**C* (color intensity)**	**Hue* angle**
80°C-1.5 m/s	42.38	30.52	29.22	42.25	42.99
80°C-0.5 m/s	48.31	30.43	29.99	42.73	43.36
60°C-1.5 m/s	38.78	33.25	26.99	42.82	40.88
60°C-0.5 m/s	38.97	32.44	31.39	45.14	43.13
40°C-1.5 m/s	37.58	27.68	28.18	39.50	43.79
40°C-0.5 m/s	45.73	30.06	31.74	43.91	44.38
Min	37.58	27.68	26.99	39.50	40.88
Max	48.31	33.25	31.74	45.14	44.38
Avg	**41.96**	**30.73**	**29.58**	**42.72**	**43.09**

5.2.3 Determination of Moisture Content

The moisture content of the dried products is targeted to be 1-10% (Source: Sahin, 2010; Ozen, 2018), and the amount of moisture to be removed is determined in Section 5.1 according to the initial moisture content measurements. The experiments are terminated when the targeted moisture content reaches. The product dried under atmospheric conditions is expected to stabilize by absorbing some moisture, and dried tomato samples taken from each experiment are brought to the laboratory two weeks after the experiments. After the samples in an oven heated to 105°C in the laboratory (Figure 5.10) reached a constant mass, their weight measurements are conducted, the moisture content is calculated, and the results are given in Table 5.8. According to the Table, the moisture content of all samples is within the reference range.

Figure 5.10. Moisture determination in the laboratory

Table 5.8. Moisture content of the dried tomatoes

	Moisture content (%)
Dried product	3-5
Reference (Özen, 2018)	1-10

5.3 Determination of Diffusion Coefficient

The diffusion coefficient of dried tomatoes varies in the range of 10^{-7}-10^{-11} m^2/s in the literature (Source: Ozen 2018). Effective diffusion coefficients (D_{eff}) are calculated according to equations in Ch.4.3 due to a decreasing velocity period due to the internal mass transfer resistance (Table 5.9). Table 5.9 shows that the diffusion coefficients increase with drying air temperature and velocity. It is seen that the diffusion coefficient is higher for the samples in the experiments performed at 80°C-1.5 m/s. Also, D_{eff} values are compatible with the literature.

The diffusion coefficient is a measure of the mobility of the substance in its medium. The drying temperature significantly affects the internal mass transfer during drying because the higher the drying temperature, the higher the moisture diffusion rate from the interior areas to the surface. Since most of the drying mechanism is vapor diffusion, surface water removal is faster at a higher temperature. The diffusion coefficient is directly proportional to the temperature (Source: Rajkumar, 2007). The diffusion coefficient also increases with air velocity (Source: Akhijani et al., 2016). These effects are seen in both Table 5.9 and Figure 5.11.

Table 5.9. Effective diffusion coefficient values for experimental conditions

Experimental conditions		
Temperature (°C)	**Air velocity (m/s)**	**D_{eff} (m^2/s)**
40	0.5	$1.63x10^{-7}$
	1.5	$2.03x10^{-7}$
60	0.5	$2.24x10^{-7}$
	1.5	$2.98x10^{-7}$
80	0.5	$2.86x10^{-7}$
	1.5	$5.34x10^{-7}$

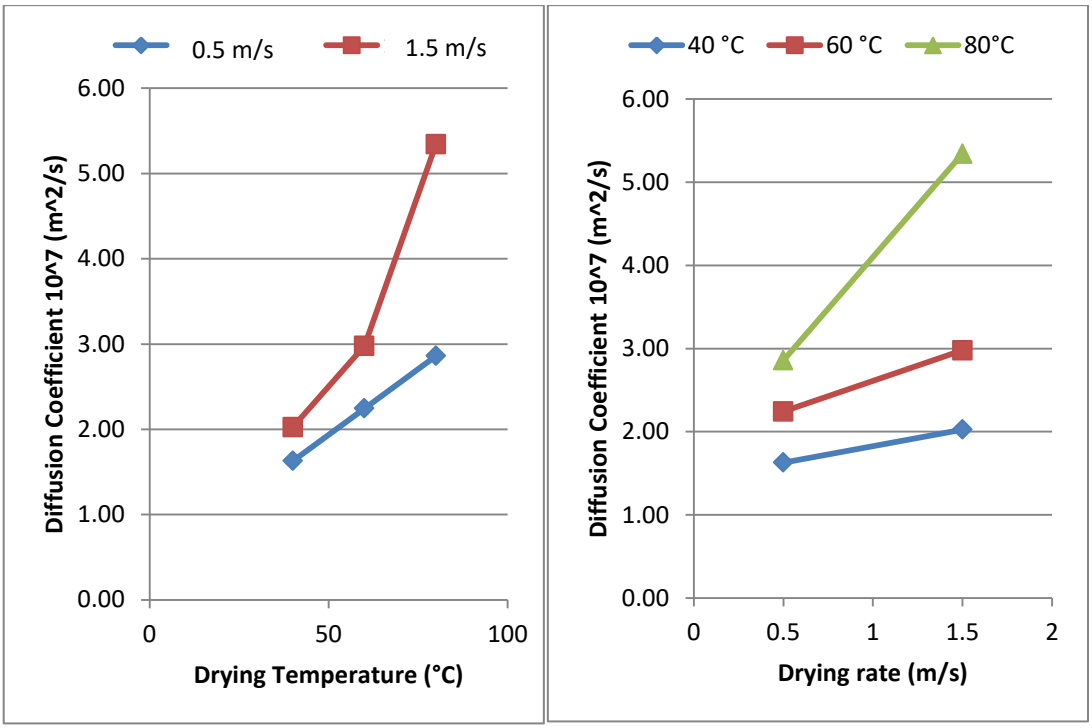

(a) (b)

Figure 5.11. Diffusion coefficient change with (a) temperature at different velocities, (b) velocity at different air temperatures

5.4 Thin Layer Drying Curve Modeling

M values are converted to the more useful dimensionless MR based on Equation 4.2. MR values are fitted to 10 different thin-layer models by applying nonlinear regression analysis, and the results are listed in Table 5.10. R^2, SSE, and RMSE are used for the adequacy of model fit. Here are the points to consider in order to choose the best model:

- The model with the highest R^2 value is the most compatible.
- The model with the lowest SSE value is the most compatible.
- The model with the lowest RMSE value is the most compatible.

When all parameters are evaluated, Midilli et al. determined the most suitable models to describe tomato slices' thin layer drying behavior. In the literature; on tomatoes; Page, Modified Page, and Midilli et al. are the models that represent tomato drying process best (Source: Taheri-Garavand et al., 2011; Hussein et al., 2016).

Table 5.10. Thin-layer model results for tomato drying experiments

Model	T (°C)	V (m/s)	Coefficients	R^2	SSE	RMSE
Newton	40	0.5	k= 0.006	0.965	0.04491	0.06390
		1.5	k= 0.009	0.991	0.00939	0.03065
	60	0.5	k= 0.008	0.972	0.04139	0.05643
		1.5	k= 0.01	0.97	0.02592	0.05692
	80	0.5	k= 0.009	0.945	0.05938	0.07706
		1.5	k= 0.018	0.966	0.03327	0.06449
Page	40	0.5	k=0.001 n=1.429	0.999	0.00062	0.00833
		1.5	k=0.004 n=1.164	0.999	0.00135	0.01301
	60	0.5	k=0.001 n=1.335	0.994	0.00830	0.02746
		1.5	k=0.002 n=1.307	0.991	0.00728	0.03483
	80	0.5	k=0.001 n=1.498	0.991	0.00938	0.03424
		1.5	k=0.003 n=1.442	0.999	0.00121	0.01418
Log.	40	0.5	a=1.4 k=0.004 c=-0.359	0.994	0.00807	0.02994
		1.5	a=1.157 k=0.007 c=-0.145	0.999	0.00095	0.01089
	60	0.5	a=1.703 k=0.003 c=-0.701	0.999	0.00077	0.00837
		1.5	a=1.869 k=0.004 c=-0.875	0.999	0.00026	0.00660
	80	0.5	a=3.22 k=0.002 c=-2.216	0.999	0.00037	0.00677
		1.5	a=1.47 k=0.01 c=-0.445	0.997	0.00286	0.02181
Two term	40	0.5	a=0.613 k0=0.006 b=0.464 k1=0.006	0.978	0.09916	0.02835
		1.5	a=0.513 k0=0.01 b=0.525 k1=0.01	0.994	0.10021	0.00645
	60	0.5	a=0.531 k0=0.008 b=0.53 k1=0.008	0.978	0.08936	0.03199
		1.5	a=0.769 k0=0.01 b=0.277 k1=0.01	0.975	0.10906	0.02173
	80	0.5	a=0.552 k0=0.01 b=0.526 k1=0.01	0.957	0.09928	0.04662
		1.5	a=0.662 k0=0.019 b=0.407 k1=0.019	0.973	0.11576	0.02601
Henderson & Pabis	40	0.5	a=1.077 k=0.006	0.978	0.02836	0.05326
		1.5	a=1.038 k=0.01	0.994	0.00645	0.02677
	60	0.5	a=1.061 k=0.008	0.978	0.03202	0.05165
		1.5	a=1.046 k=0.01	0.975	0.02167	0.05564
	80	0.5	a=1.078 k=0.01	0.957	0.04669	0.07203
		1.5	a=1.07 k=0.019	0.973	0.02602	0.06097

Cont. of the next page..

.

...Cont. of the Table 5.10.

Modified Page	40	0.5	n=1.429 k=0.006	0.999	0.00062	0.00833
		1.5	n=1.164 k=0.008	0.999	0.00135	0.01301
	60	0.5	n=1.335 k=0.007	0.994	0.00830	0.02746
		1.5	n=1.307 k=0.01	0.991	0.00728	0.03483
	80	0.5	n=1.498 k=0.01	0.991	0.00938	0.03424
		1.5	n=1.442 k=0.018	0.999	0.00121	0.01418
Approximation of diffusion	40	0.5	a=1.94 k=0.009	0.998	0.00212	0.01456
		1.5	a=1.692 k=0.013	0.991	0.00139	0.01244
	60	0.5	a=1.848 k=0.011	0.993	0.01023	0.02919
		1.5	a=1.821 k=0.015	0.99	0.00819	0.03420
	80	0.5	a=1.953 k=0.015	0.986	0.01492	0.04072
		1.5	a=1.964 k=0.028	0.997	0.00318	0.02131
Wang &Singh	40	0.5	a=-0.004 b=4.5E-0.6	0.993	0.00868	0.02946
		1.5	a=-0.007 b=1.4E-0.5	0.999	0.01320	0.01211
	60	0.5	a=-0.005 b=6.1E-06	0.999	0.00055	0.00677
		1.5	a=-0.007 b=1.1E-05	0.999	0.00045	0.00798
	80	0.5	a=-0.006 b=4.9E-06	0.999	0.00037	0.00638
		1.5	a=-0.013 b=4.1E-05	0.998	0.00226	0.01799
Modified Henderson &Pabis	40	0.5	a=0.414 k=0.006 b=0.395 g=0.006 c=0.268 h=0.006	0.978	0.05142	0.07171
		1.5	a=0.356 k=0.01 b=0.356 g=0.01 c=0.326 h=0.01	0.994	0.05491	0.07811
	60	0.5	a=0.418 k=0.008 b=0.559 g=0.008 c=0.085 h=0.008	0.978	0.01500	0.03535
		1.5	a=0.352 k=0.01 b=0.363 g=0.01 c=0.331 h=0.01	0.975	0.00784	0.03346
	80	0.5	a=0.346 k=0.01 b=0.36 g=0.1 c=0.372 h=0.01	0.957	0.00284	0.01776
		1.5	a=0.213 k=0.019 b=0.318 g=0.019 c=0.538 h=0.019	0.973	0.02830	0.06358
Midilli et.al..	40	0.5	a=0.976 k=0.001 n=1.519 b=-0.0002	0.999	0.00014	0.00453
		1.5	a=1.027 k=0.008 n=1.022 b=-0.0003	0.999	0.00057	0.00973
	60	0.5	a=0.972 k=0.002 n=1.189 b=-0.0007	0.999	0.00062	0.00829
		1.5	a=0.982 k=0.005 n=1.044 b=-0.0016	0.999	0.00020	0.00710
	80	0.5	a=0.991 k=0.002 n=1.147 b=-0.0019	0.999	0.00030	0.00712
		1.5	a=1.004 k=0.005 n=1.313 b=-0.0006	0.999	0.00007	0.00430

Linear regression analysis is applied to the Midilli et.al. model to determine the effect of the coefficients to the model. The obtained equations of the coefficients and R^2 values are given in Table 5.11.

Table 5.11. Linear regression analysis results

Model	Coefficient	Equation	R^2
Midilli et.al..	a	a=0.025v-0.0001T+0.973	0.437
	k	k=0.004v-0.000025T+0.001	0.837
	n	n=(-0.159)v-0.001T+1.425	0.227
	b	b=0.0001v-0.000025T+0.001	0.411

5.5 Energy and Exergy Analysis

Energy and exergy analysis to obtain EU and EUR of the drier are conducted by EES software (EES Inc., 2012) using the Eq.s given in Sections 4.5.1 and 4.5.2.. The temperature, relative humidity, enthalpy, and entropy values, and energy and exergy content at each state (Figure 4.15) of the dryer are given Table 5.12. Dead state values are taken as T_0=22°C, P_0=101.325 kPa. Table 5.13 gives the EU EUR, SMER and exergy efficiency and exergy destruction values of each component. In addition, the inlet-outlet temperatures of the geothermal fluid to the heat exchanger, the air velocity, and the power values of the fan are given in the same table. The most significant exergy destruction occurs in the fan, heat exchanger, and the drying chamber. Depending on the exergy destruction, the exergy efficiency is the highest in the drying chamber and the lowest in the fan. Looking at the EU values, it can be said that the minimum energy consumption is in the 40°C-0.5m/s experiment and the maximum energy consumption is in the 60°C-1.5m/s experiment. The increase in drying air temperature and velocity causes an increase in energy consumption. The same results can be drawn for the EUR values while the highest SMER value is seen in the 40°C-0.5m/s experiment, and the lowest SMER value is seen in the 60°C-1.5m/s experiment. Also, the SMER value increases as the temperature increases at constant drying air velocity but decreases as the air velocity increases at constant drying temperature.

These calculations are applied only for the experiments at 40 and 60°C because the maximum operation temperature of the temperature and velocity sensors used inside the drier is 60°C.

Table 5.12. Energy and exergy analysis data of the drier

Experimental condition	State	T (K)	RH (%)	Enthalpy (kJ/kg)	Entropy (kJ/kgK)	Energy (kW)	Exergy (kW)
40°C-0.5 m/s	0	295.15	42	39.64	5.685	-	-
	1	290	50.6	30.81	5.667	5.88	0.0091
	2	294.2	90.7	56.25	5.682	10.74	0.0003
	3	313.8	29.6	77.5	5.747	14.80	0.1115
	4	311.7	33.1	75.35	5.74	14.39	0.0884
40°C-1.5 m/s	0	295.15	42	39.64	5.685	-	-
	1	308.5	56.1	82.52	5.73	46.5495	0.3327
	2	311.4	43.19	85.5	5.739	48.2306	0.2516
	3	316.8	32.3	91.2	5.757	51.4459	0.4455
	4	314.7	36.1	89	5.75	50.2049	0.3542
60°C-0.5 m/s	0	295.15	42	39.64	5.685	-	-
	1	310.6	48.4	85.63	5.737	15.4477	0.1322
	2	315.6	35.02	90.88	5.753	16.3948	0.1277
	3	329.9	17.2	105.7	5.797	19.0683	0.3567
	4	325	21.8	100.62	5.782	18.1518	0.2656
60°C-1.5 m/s	0	295.15	42	39.64	5.685	-	-
	1	271.2	57.7	54.14	5.6	29.0136	1.138
	2	325.5	25.42	111	5.784	59.4849	0.822
	3	331.3	19.3	117.1	5.802	62.7539	1.149
	4	327.8	22.8	113.41	5.791	60.7764	0.943

Table 5.13. EU, EUR, SMER and exergy destruction rates of the drier components

Experimental condition		40°C-0.5 m/s	40°C-1.5 m/s	60°C-0.5 m/s	60°C-1.5 m/s
T_{wi}	(K)	355.4	347.9	355.7	352.4
T_{wo}	(K)	313.6	308.4	322.6	315.2
m_w	(kg/s)	0.022	0.019	0.019	0.021
W_{fan}	(kW)	0.862	2.313	0.97	31.1
eff_{fan}	(%)	1.2	3.5	1	1.1
eff_{hex}	(%)	4.7	34.2	11.95	47.24
eff_{dc}	(%)	79.23	81.7	74.47	82.12
EU	(kW)	0.41	1.245	0.9218	1.966
EUR	(%)	10.12	38.69	34.4	60.87
$EX_{dest.dc}$	(kW)	0.0232	0.0814	0.0911	0.205
$EX_{dest.hex}$	(kW)	0.471	0.4291	0.3871	0.546
$EX_{dest.fan}$	(kW)	0.871	2.394	0.9748	31.42
SMER	(kg/kW.h)	2.467	1.738	3.845	0.311

5.6 CFD Modelling

The drying process is also modelled using Comsol Multiphysics software. The model is validated and simulated for experimental conditions. Finally, both model and experimental results are compared.

5.6.1 Validation

The CFD model of the drying process is developed based on the Section 4.7 using COMSOL Multiphysics software. It is assumed that there is only a single slice of tomato at the base of the dryer (Figure 4.16). The model is validated with experimental MR data. The validation results are presented in Table 5.14 and Figure 5.12. It can be seen from the Table and the Figure that the MR values obtained from the model are in good agreement with the experimental data for 40°C-0.5 m/s, 40°C-1.5 m/s, 60°C-0.5 m/s, 60°C-1.5 m/s and 80°C-1.5 m/s. The difference between experimental data and model results are 10-16% which is compatible with the literature (Source: Doymaz, 2004; Gonzalez 2012; Frost, 2017; Belay, 2020). Model results and experiments conducted at 80°C-0.5 m/s have a difference as high as 35% which is higher than acceptable rates.

Table 5.14. Validation of the CFD model using moisture ratio data

40°C-0.5 m/s			**40°C-1.5 m/s**		
Time (min)	**Moisture ratio (%)**		**Time (min)**	**Moisture ratio (%)**	
	Simulation results	**Experimental results**		**Simulation results**	**Experimental results**
0	1	1	0	1	1
15	0.897	0.959	15	0.737	0.879
30	0.802	0.906	30	0.611	0.743
45	0.739	0.852	45	0.542	0.605
60	0.635	0.799	60	0.482	0.481
90	0.547	0.678	90	0.399	0.363
120	0.442	0.552	120	0.339	0.286
150	0.397	0.435	150	0.281	0.233
180	0.358	0.34	180	0.226	0.201
240	0.255	0.186	210	0.177	0.161
300	0.115	0.102	240	0.135	0.143
360	0.058	0.053	Cont. of the next page...		

...Cont. of the Table 5.14.

60°C-0.5 m/s			60°C-1.5 m/s		
Time (min)	Moisture ratio (%)		Time (min)	Moisture ratio (%)	
	Simulation results	Experimental results		Simulation results	Experimental results
0	1	1	0	1	1
15	0.853	0.919	15	0.868	0.885
30	0.790	0.846	30	0.748	0.784
45	0.728	0.770	45	0.638	0.697
60	0.635	0.707	60	0.531	0.602
90	0.536	0.578	90	0.401	0.455
120	0.423	0.463	120	0.256	0.300
150	0.279	0.349	150	0.133	0.164
180	0.225	0.251	180	0.054	0.058
195	0.200	0.205			
210	0.176	0.148			
225	0.155	0.121			
240	0.076	0.081			
255	0.052	0.067			

80°C-0.5 m/s			80°C-1.5 m/s		
Time (min)	Moisture ratio (%)		Time (min)	Moisture ratio (%)	
	Simulation results	Experimental results		Simulation results	Experimental results
0	1	1	0	1	1
15	0.676	0.912	15	0.755	0.851
30	0.545	0.819	30	0.571	0.662
45	0.458	0.738	45	0.402	0.496
60	0.403	0.640	60	0.286	0.345
75	0.357	0.568	75	0.225	0.238
90	0.313	0.480	90	0.173	0.143
120	0.235	0.328	105	0.107	0.072
150	0.168	0.168	115	0.055	0.043
165	0.141	0.118			
180	0.061	0.048			

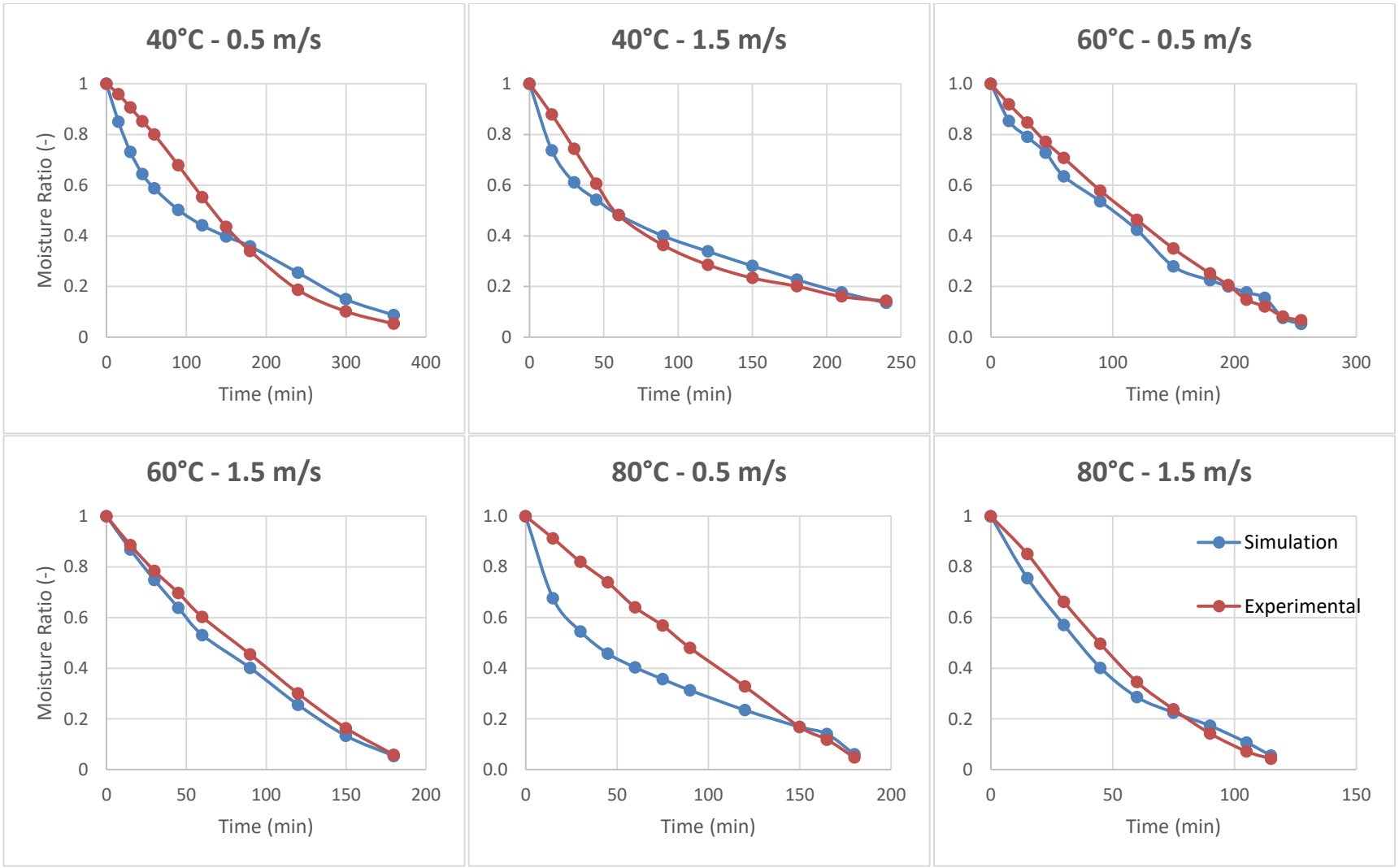

Figure 5.12. Validation of experimental and simulation data for moisture ratio and drying time at different air temperatures and velocities

5.6.2 CFD Analysis

Air Velocity Analysis

The validated model is simulated for each experimental air temperature and velocity conditions and drying time results are presented in Figure 5.13. The air velocity is near zero at the cabin's edges, as expected. The air velocity increases towards the middle of the cabin and has the maximum velocity in the middle which is 0.7 m/s for 0.5 m/s simulations and 2 m/s for 1.5 m/s simulations.

The air flow is not affected because there is a single slice of tomato in the dryer without a tray. Similar behavior is observed in Villa-Corrales et al. (2010) and Belay (2020).

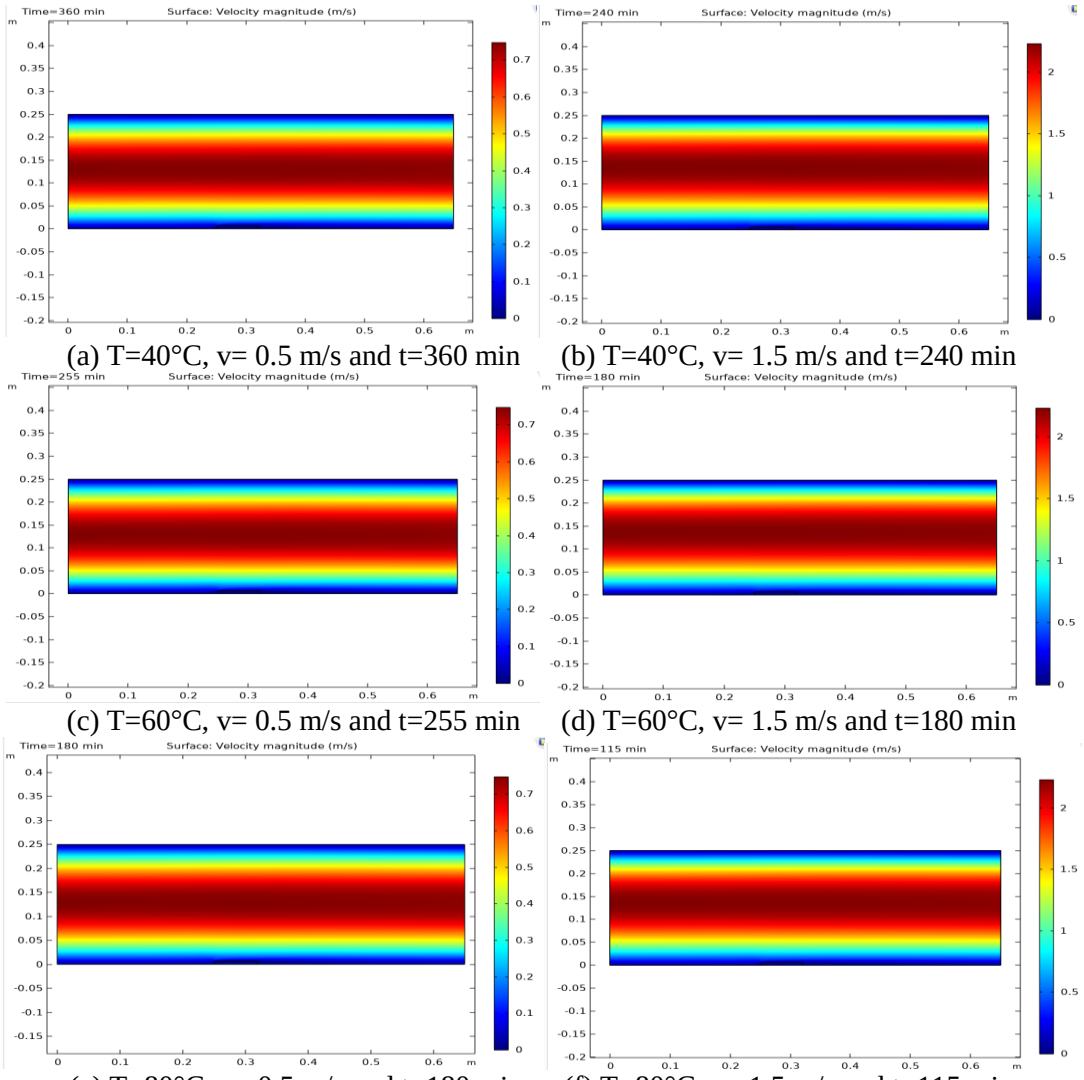

(a) T=40°C, v= 0.5 m/s and t=360 min (b) T=40°C, v= 1.5 m/s and t=240 min

(c) T=60°C, v= 0.5 m/s and t=255 min (d) T=60°C, v= 1.5 m/s and t=180 min

(e) T=80°C, v= 0.5 m/s and t=180 min (f) T=80°C, v= 1.5 m/s and t=115 min

Figure 5.13. Air velocity distributions at different air temperatures and velocities

Moisture Content Analysis of Tomato Slice

Moisture content change within the tomato slice with time is shown in Figure 5.14. As can be seen from the Figure, the tomato slice has 100% moisture content at the beginning of the drying process (at the moment of zero). Once hot air flow is introduced, the moisture content of the tomato slice begins to decrease. The decrease in the moisture content of tomato slice is not evenly distributed on each surface. The amount of the moisture on the surface that meets the air is always the driest compared to other surfaces. For example, in the 40°C-0.5 m/s experiment, the front surface moisture content reached 0 at the 180th minute, but the rear surface is close to 70% (Figure 5.14a). At the end of the experiment, the moisture content on all surfaces is zero except for the bottom surface. In addition, similar results are observed at the end of other experiments. This is because the desired final moisture content is within a specific range. Similar phenomenon is observed in most previous works (Source: Villa-Corrales et al., 2010; Belay, 2020).

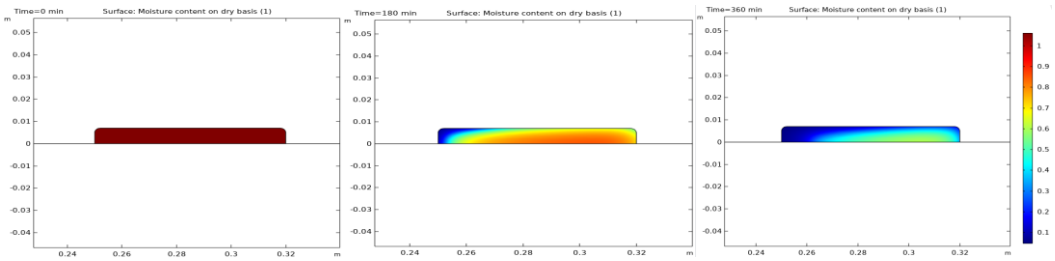

(a) T=40°C, v= 0.5 m/s and t=0;180;360 min

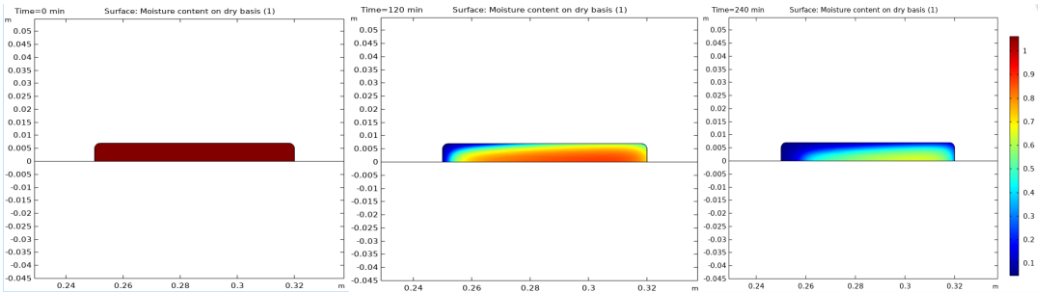

(b) T=40°C, v= 1.5 m/s and t=0;120;240 min

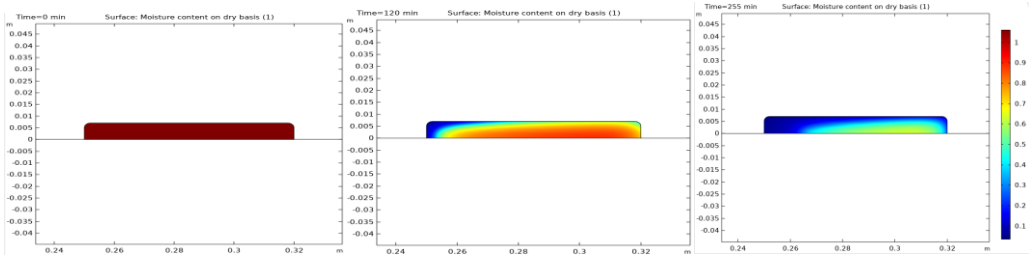

(c) T=60°C, v= 0.5 m/s and t=0;120;255 min

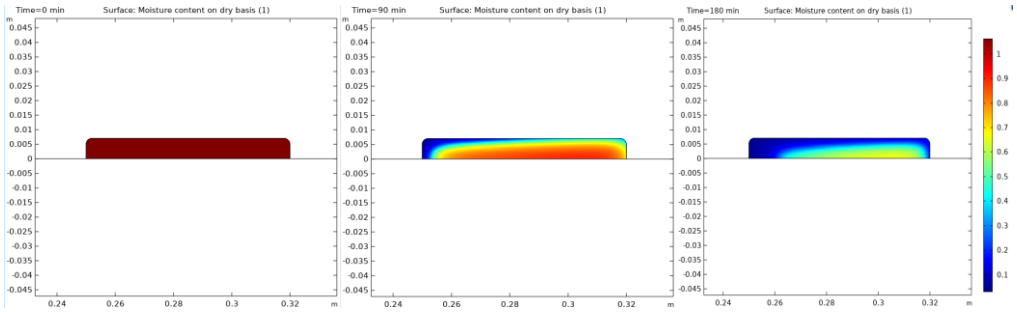

(d) T=60°C, v= 1.5 m/s and t=0;90;180 min

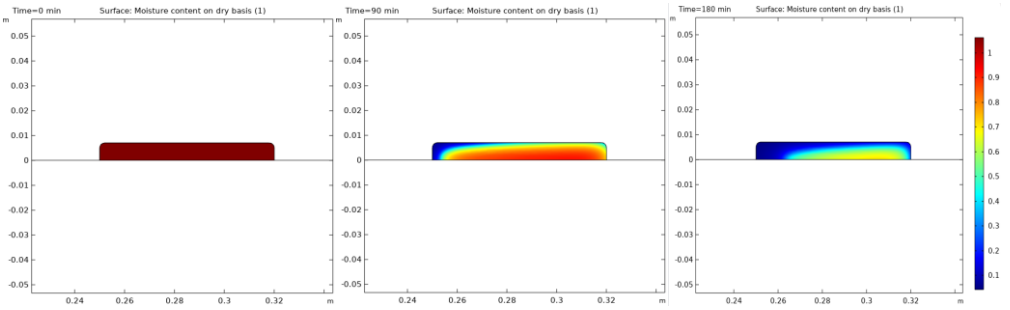

(e) T=80°C, v= 0.5 m/s and t=0;90;180 min

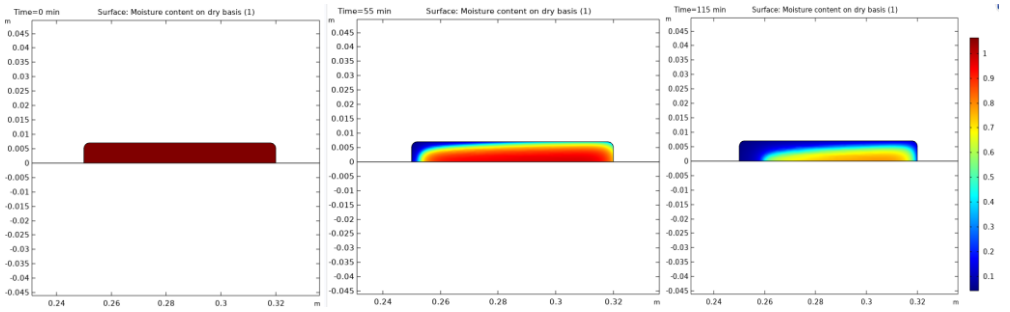

(f) T=80°C, v= 1.5 m/s and t=0;55;115 min

Figure 5.14. Moisture content of tomato slice simulations with time under different air temperatures and velocities

Dryer Cabinet and Tomato Slice Temperature Analysis

Figure 5.15 shows the temperature change of the dryer cabinet and the tomato slice with time at different air temperatures and velocities. The air temperature and the tomato slice temperature are constant at the beginning of the drying process (at the moment of zero) and are at room temperature. After a stream of hot air is introduced, the inlet temperature began to rise, and after a while, the entire temperature in the cabin became almost equal and at the desired temperature (40-60-80°C). However, the temperature of the part left behind the tomato slice is lower under any circumstances. The temperature change indicates that the temperature around the slice is lower due to the heat transfer from the air to the tomato slice.

The decrease in the temperature of the tomato slice is not evenly distributed on every surface. The surface temperature of the tomato slice in the direction from which the air comes is always the hottest compared to other surfaces. For instance, while the front surface temperature is 28°C in the 180th minute for 40°C-0.5 m/s, it reached approximately 35°C at the end of the drying time. The front surface temperature of the tomato slice is determined as approximately 55°C and 77°C for drying air temperature of 60°C and 80°C, respectively. However, the back surface of the tomato slice is close to room temperature throughout the drying period for every condition. The cabin temperature in the drying experiments performed with an air velocity of 0.5 m/s reaches the desired temperature in a longer time compared to the drying experiments performed with an air velocity of 1.5 m/s. No temperature change can be observed except for the parts of the cabinet close to the tomato. This is because the tomato has a minimal surface and is located at the base. The same observations are encountered by Zadin et al. (2015), Villa-Corrales et al.(2010), Belay (2020).

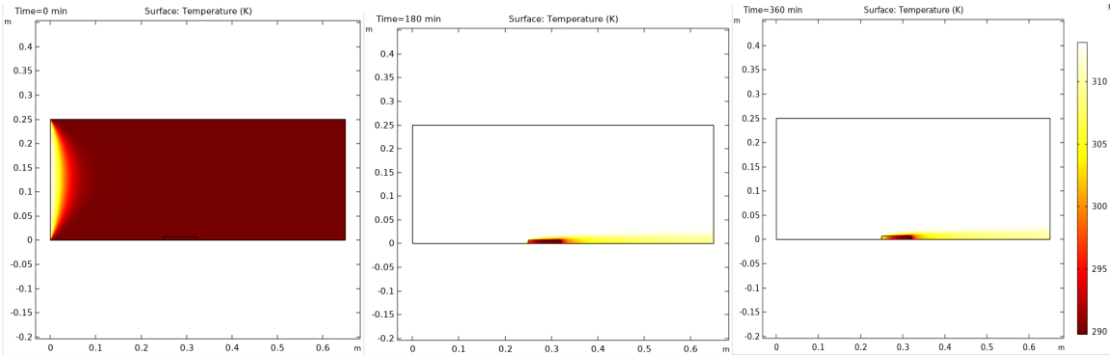

(a) T=40°C, v= 0.5 m/s and t=0;180;360 min

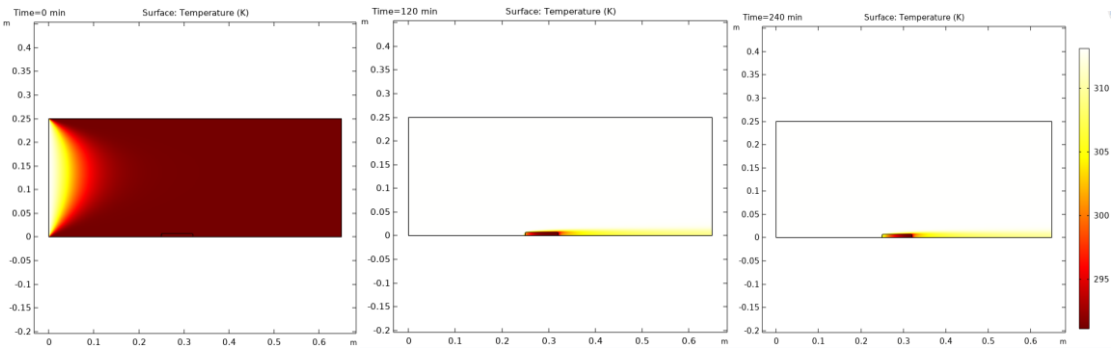

(b) T=40°C, v= 1.5 m/s and t=0;120;240 min

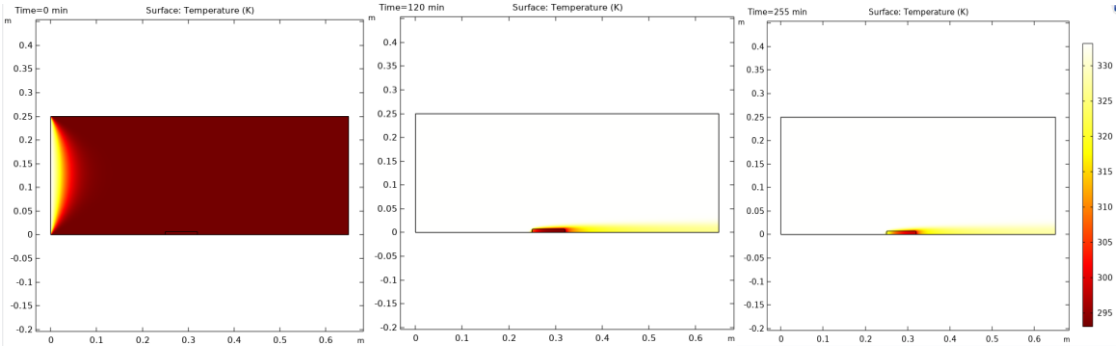

(c) T=60°C, v= 0.5 m/s and t=0;120;255 min

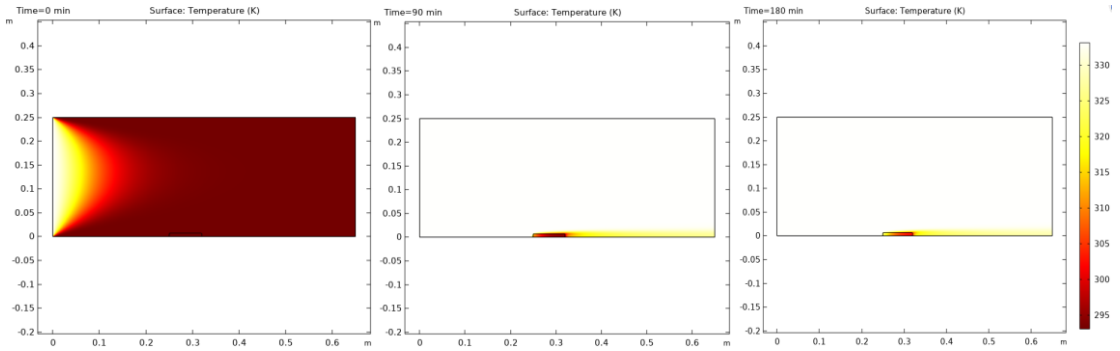

(d) T=60°C, v= 1.5 m/s and t=0;90;180 min

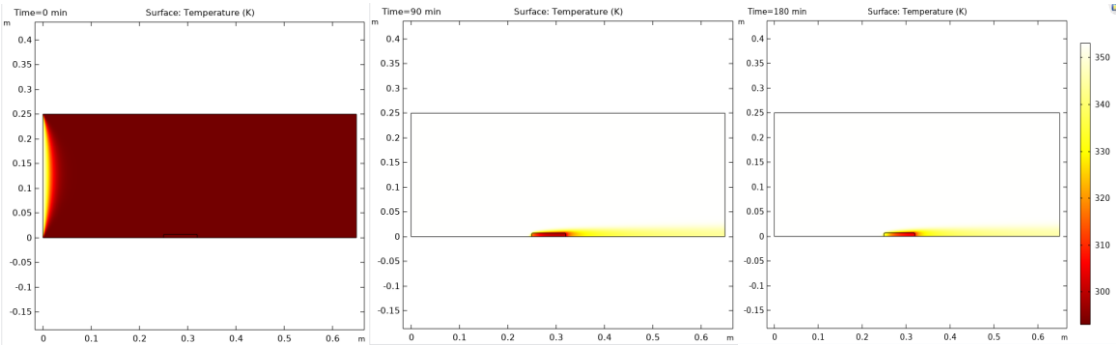

(e) T=80°C, v= 0.5 m/s and t=0;90;180 min

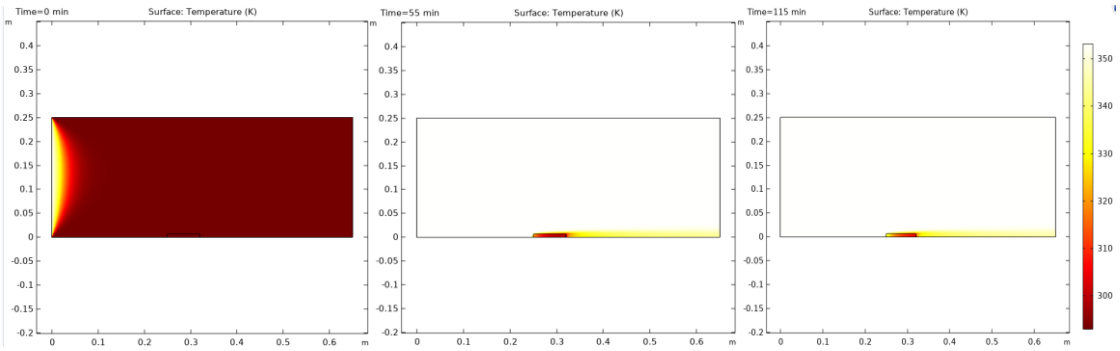

(f) T=80°C, v= 1.5 m/s and t=0;55;115 min

Figure 5.15. Temperature simulations with time for different air temperatures and velocities

CHAPTER 6

CONCLUSIONS

The aim of this Thesis is to examine the effects of drying air temperature and velocity on dried tomatoes based on the quality parameters The study is conducted in two parts: experiments and CFD modelling. The geothermal sourced cabinet type drier used in the experimental part, is installed in a heat center of BNGDHS. During experiments, the effects of drying air temperature (40-60-80°C) and velocity (0.5-1.5 m/s) on the drying process and product quality are evaluated. The air temperature, relative humidity and velocity data collected during the experiments. Those data are also used for energy and exergy analysis of the drier to evaluate thermodynamic performance of the drier.

Some concluding remarks which can be extracted from the experimental part of the Thesis are as follows:

- The drying time for experiments; varies between 115 and 360 minutes. The results showed that as the drying air temperature and velocity increase, the drying rate and, accordingly, the drying time decrease.

- Practical moisture diffusion values; tomatoes are in the range of $1.63*10^{-7}$-$5.34*10^{-7}$ m^2/s, and literature data is in the range of 10^{-7}-10^{-11} m^2/s.

- In order to describe the drying kinetics of tomato slices, thin layer models suitable for tomatoes in the literature are applied to dimensionless moisture content data. The results of nonlinear regression analysis showed that Midilli et al. for tomatoes are the best models to describe the drying behavior.

- The average pH values of dry products are 4.38 in tomatoes, and the literature data is in the range of 4-4.5. This means that the dried tomato slices in the result of all experimental conditions give the appropriate result in terms of pH values.

- Hue angle and saturation are evaluated 80°C-0.5 m/s under the conditions of an experiment that is performed in the color values, so determined to have examples of best-dried tomatoes with high brightness and redness.

- Dry product moisture determination values are between 3-5% in tomatoes, and literature data is 1-10% in the range. In other words, dried tomato slices as a result of all experimental conditions give appropriate results in terms of moisture determination values.

- In all experiments, the greatest exergy loss occurs in the fan, and the heat exchanger and drying chamber are in the second and third rows.

- According to EU values, it can be said that the minimum energy consumption is in the 40°C-0.5 m/s experiment and the maximum energy consumption is in the 60°C-1.5 m/s experiment.

- The highest SMER and EUR values are seen in the 40°C-0.5 m/s experiment, and the lowest SMER and EUR values are seen in the 60°C-1.5 m/s experiment.

- Reusing air improves the dryer's performance. In geothermal dryers, since the energy source is geothermal fluid, it is almost free. However, if the energy source is a fossil fuel, the drying process is more profitable regarding energy and exergy efficiency.

The study can be safely used for further practical applications and as a theoretical basis for analyzing the food drying process.

The drier is modelled using COMSOL Multiphysics software including a single slice of tomato. If the entire tray loaded with tomato slices would be modelled, the drying time would increase towards the outlet boundary since the slice behind each slice would be affected by the lower temperature and each slice would be affected by the moisture flow caused by the slice drying in front of it. This model would provide a better understanding of heat and moisture transport within the sample.

During the drying experiments, many limitations can be encountered such as;

- the MR distribution inside the tomato slice cannot be observed.
- the temperature change of the tomato slice cannot be observed.
- measurement of drying air temperature and velocity change with time in the cabinet requires a high amount of sensors and time.

CFD models can not replace the measurements but the amount of experimentation and the overall cost can be significantly reduced. A quantitative prediction for any parameter change with space and time can be obtained by CFD analysis. A CFD model is a powerful tool which leads to a better understanding of the drying process observing the changes in MR, temperature and velocity in the cabinet and also within the tomato slice. These observations help to modify the experimental conditions in order to obtain the best drying air conditions, and to improve the drier components. Therefore, instead of using a limited number of experiments, experiments accompanied with CFD analysis would give more efficient and reliable results in the drying studies. In the Thesis, the conclusions drawn from experiments plus CFD modeling couple are;

- Trays in the cabinet can be placed in different positions for a better drying process,
- Dryer dimensions can be changed for a more efficient drying,
- Changes in the drying process can be observed better with 3D modeling.

During experiments, some withdrawals are encountered with the drier. Suggestions to overcome these withdrawals for further studies are;

- Since the system is controlled manually, keeping the drying air parameters constant is challenging. The automation system will increase the stability of the parameters.
- The dryer length should be increased due to the difficulty of achieving stable conditions at higher drying air velocities. The number of trays should be increased to determine the optimum dryer length.
- The products should be weighed in the dryer. Because removing, putting weight and back causes temperature drop and moisture gain in the product.

REFERENCES

Abak, K., 2010, “Türkiye’de Domatesin Dünü, Bugünü Ve Yarını”, Faculty of Agricultural Sciences, University of European Lefke, Turkish Seed Growers Association.

Abdullah, K., Gunadnya, I., 2010, “Use Of Geothermal Energy For Drying And Cooling Purposes”, Proceedings World Geothermal Congress 2010, Bali, Indonesia.

Acikders.ankara.edu.tr/mod/resource/view.php?id=3001&forceview=1.

Acikders.ankara.edu.tr/mod/resource/view.php?id=3002&forceview=1.

Ahmed, N., Singh, J., Chauhan, H., Kour, H., 2013, “Different Drying Methods: Their Applications and Recent Advances”, International Journal of Food Nutrition and Safety, 4(1): 34-42.

Akanbi, C., Adeyemi, R.S., Ojo, A., 2006, “Drying Characteristics And Sorption Isotherm Of Tomato Slices”, Journal Of Food Engineering 73(2):157-163.

Akhijani, H.S., Arabhosseini, A., Kianmehr, M.H., 2016, “Effective Moisture Diffusivity During Hot Air Solar Drying Of Tomato Slices”, Vol. 62, (1): 15–23.

Aktas,M., Menlık,T., Boran,K., Aktekelı,B., Aktekelı,Z., 2014, “Drying Orange Peel in a Heat Pump Dryer”, Design And Technology, GU J Sci Part:C, 2(2):229-238.

Andritsos, N., Dalampakis, P., Kolios, N., 2003 “Use Of Geothermal Energy For Tomato Dryıng”, Chemical Process Engineering Research Institute, Greece and Dept. of Mechanical &Industrial Engineering, University of Thessaly, Greece.

Appoldt, Y., and Raihani G., 2017, “Determining Moisture Content”.

Ashebır, D., Jezık, K., Weıngartemann, H., Gretzmacher, R., 2009, “Change in Color And Other Fruit Quality Characteristics Of Tomato Cultivars After Hot-Air Drying At Low Final-Moisture Content”.

Atlasbig.com/en-us/countries-tomato-production, 2022.

Ayan, H., 2010, “Güneste Ve Yapay Kurutucuda Kurutulmus Domates (Lycopersitcum Esculentum) Üretim Ve Proses Sırasındaki Degişimlerin Belirlenmesi”.

Ayaydın, E., 2022, “Türkiye'den 54 Ülkeye 363,3 Milyon Dolarlık Domates İhracatı”.

Bagheri, H., Arabhosseini, A., Kianmehr, M. H., Chegini, G. R., 2013, “Mathematical Modeling Of Thin Layer Solar Drying Of Tomato Slices”, Vol. 15, No.1.

Bahadori, A., 2016, “Solids Handling Systems And Dryers, in Essentials Of Oil And Gas Utilities”.

Basak, H., Madakbaş, S.Y., Gürdal, B., 2014, “Feasibility Of Vegetable Drying Technic By Geothermal Heating At City Of Kirsehir”, Turkish Journal Of Agricultural And Natural Sciences, Special Issue: 1.

Bashimov, G., 2016, “Türkiye’nin Domates İhracat Performansı Ve Rakabet Gücü”,Ömer Halisdemir Üniversitesi, Sosyal Bilimler Enstitüsü, Niğde .

Baysal T., Ozbalta N., et al., 2015, “Investıgatıon Of Effects Of Varıous Dryıng Methods On The Qualıty Characterıstıcs Of Apple Slıces And Energy Effıcıency”, Journal of Thermal Science and Technology.

Belay, A. 2020, “Modelıng and Sımulatıon of Heat And Mass Transfer in Ethiopian Fresh Injera Drying Process”, Master Thesis.

Belice, T., Yüksel, A., Akçiçek, S.F., 2020, “Importance of Dried Fruits and Vegetables in the Older Adults” , 2(2):28-35.

Blabmarket.Com/Urun/Ph-Olcer-Et-Peynir-Sut-Ph-Metre-Mw102-Food-Milwaukee.

Carlos, J., Bilgin, E., 2022, “Prices of Turkish Tomato Soar Despite Export Limitation Measures”, Tridge Analysis.

Cetin,N., “Effect of Drying Conditions on Color Properties of Apples and Oranges”, European Journal of Science and Technology, No. 17, pp. 463-470, December 2019, EJOSAT.

COMSOL Multiphysics 5.5, Evaporation in Porous Media with Large Evaporation Rates

COMSOL Multiphysics 5.5, Vacuum Drying

Corrêa, P.C., Oliveira, G.H., Baptestini, F.M., Diniz, M.D.M., Chılean, A., 2012, "Tomato Infrared Dryıng: Modelıng And Some Coefficıents Of The Dehydratıon Process", Journal Of Agrıcultural Research 72(2).

Day, M.A., 2004, "The no-slip condition of fluid dynamics", Erkenntnis, 33 (3): 285–296.

Demiray, E., Tulek, Y., 2008, "Domates Kurutma Teknolojisi Ve Kurutma Isleminin Domatesteki Bazı Antioksidan Bilesiklere Etkisi", (3) 9-20.

Denge,A., 2011, "Investigation of Physical Changes in the Structure of Quince During Drying", Department of Food Engineering.

Dikbasan, T., 2007, "Determınatıon Of Effectıve Parameters For Dryıng Of Apples".

Doran, P.M., 2013, "Bioprocess Engineering Principles (Second Edition)".

Doymaz, I. , 2007, "Air Drying Characteristics Of Tomatoes", Journal Of Food Engineering, 78, 1291-1297.

Doymaz, I., 2008, "Convective Drying Kinetics Of Strawberry", Chemical Engineering And Processing, 47, 914-919.

Doymaz, I.,2010, "Evaluation Of Mathematical Models For Prediction Of Thin-Layer Drying Of Banana Slices", International Journal Of Food Properties, 13, 486-497.

Doymaz,I., 2004, "Convective Air Drying Characteristics of Thin Layer Carrots", Journal of Food Engineering,61, 359-364.

Earle, R.L., 1983, "Unit Operations in Food Processing", Pergamon Press, 207 pages.

Enkurmakine.Com.Tr/Doner-Kurutucular/.

Environmental-Expert.Com/Products/Hobo-Model-U12-013-Temp-Rh-2-External-Channel-Data-Logger-391645

Erdem, M., Kamıslı, F., Varol, Y., Öztop, H.F., 2021, "Energy And Exergy Analysis Of Drying Behavior For A Fish".

Ergün, A.R., Bozkır, H., Saygıner, B.N., Baysal, T., 2020, "Farklı Tuzlarla Kurutulmuş Domatesin Bazı Kalite Özelliklerinin İncelenmesi".

Faith M., 2001, "Sun Protection in Man", Strickland, in Comprehensive Series in Photosciences.

FAOSTAT (Food and Agriculture Organization of the United Nations FAO), 2019, "The State of Food and Agriculture", 978-92-5-131789-1.

Fargali, H.M., Nafeh, A.E., Fahmy, F.H., Hassan, M.A., 2008, "Medicinal Herb Drying Using a Photovoltaic Array and a Solar Thermal System", 82(12):1154-1160.

Fellows, P.J. Food Processing Technology, Principles and Practice, 3 rd Ed., CRC Press, 2009.

Filiz, C., Uysal, C., Kılıç, E., Kurt, H., 2019, "Bir Buhar Kazanının Enerji Ve Ekserji Analizi Yoluyla Performansının Değerlendirilmesi".

Frost, J., 2017, "Standard Error of the Regression vs. R-squared"

Gao, K., Zhou, L., Bi, J., Yi, J., Wu, X., Zhou, M., ... & Liu, X. (2017), "Evaluation of browning ratio in an image analysis of apple slices at different stages of instant controlled pressure drop-assisted hot-air drying (AD-DIC)", Journal of the Science of Food and Agriculture, 97(8), 2533-2540.

Garau, M. C., Simal, S., Rossello, C., & Femenia, A. (2007), "Effect of air-drying temperature on physico-chemical properties of dietary fibre and antioxidant capacity of orange (Citrus aurantium v. Canoneta) by-products", Food chemistry, 104(3), 1014-1024.

Garg, H.P., Kumar, R., 2001, “Developments in solar drying”, Proceedings of the Second

Gavrila, C., Ghiaus, A.G., Gruia, I., 2008, “Heat And Mass Transfer in Convective Drying Processes”, Excerpt From The Proceedings Of The Comsol Conference.

Geankoplis, C. J., 2003, “ Transport Processes and Separation Process Principles”, 4th Ed.,Pearson Education Inc..

Gonzalez, A.A., Torres, S.S., and Lagunas, L.L.M., 2012, “Multiphysics modeling of warm-air drying of potatoes slices” COMSOL Conference in Milan.

Guiné, R. P. (2011), “Influence of drying method on some physical and chemical properties of pears”, International journal of fruit science, 11(3), 245-255.

Gunhan, T., Yağcıoğlu, A., 2016, “Farklı Kurutma Havası Şartlarının Rio Grande Çeşidi Domatesin Kuruma Karakteristiklerine Etkilerinin Belirlenmesi”.

Helvacı, H.U., 2012, “Desıgn And Tests Of A Geothermal Dryer And Determınatıon Of Qualıty Parameters Of Drıed Product”.

Helvacı, H.U., Khan, Z.A., 2016, “Heat Transfer and Entropy Generation Analysis Of HFE 7000 Based Nanorefrigerants” .

Hill, M., 2015, “Drying Fruits and Vegetables”.

HOBO® U12-013 Data Logger Temperature/Relative Humidity/2 External Channel, Onset.

Hussein, J. B., Filli, K. B. and Oke, M. O., 2016, “Thin Layer Modelling Of Hybrid, Solar And Open Sun Drying Of Tomato Slices”, Volume 1(1), Pages 15-27.

Iqbal, S.M.J., Zaman, U., Siddiqui, S.H., Imran, M.K., 2019, “Influence of Transformational Leadership Factors on Project Success”, Pakistan Journal of Commerce and Social Sciences, Vol. 13 (1), 231-256.

Ismail, O., 2017, “Güneş Altında Kurutulmuş Havuç Dilimlerinin Rehidrasyon Kinetiğinin İncelenmesi”.

Izmir Geothermal Inc., 2021, “https://www.izmirjeotermal.com.tr/”

Jamshed, S., 2015, “Introduction to Cfd” .

Jóhannesson, T., Guðmundsdóttir, V., Einarsson, Ó.P., Brauchler, R., Lise, W., Ince, C., Vögeli, A., 2020, “Turkey –Feasibility study on the potential for geothermal district heating and coolingsystems”.

Kaushal, P., Sharma, HK., 2012, “Concept of Computational Fluid Dynamics (CFD) and its Applications in Food Processing Equipment Design”, J Food Process Technol.

Keey, R.B., 2011, “Drying”, Thermopedia, 10.1615/AtoZ.d.drying.

Khazaei, J., Daneshmandi, S., 2007, “Modeling Of Thin-Layer Drying Kinetics Of Sesame Seeds: Mathematical And Neural Networks Modeling”, International Agrophysics, 21, 335-348.

Konicaminolta.Eu/Tr/Oelcuem-Cihazlari/Ueruenler/Renk-Oelcuemue/Renk-Oelcer/Cr-400-410/Aksesuarlar.Html.

Kostoglou , M., Chrysafis, N., Andritsos, N., 2013, “Modelling Tomato Dehydration in A Tunnel Dryer Using Geothermal Energy”, Drying Technology, 31: 5–15.

Kovacı, T., Dikmen, E., Şahin, A.Ş., 2018, “Kurutma Sistemleri, Enerji Tüketimleri Ve Ürün Kalitesine Etkileri Ve Örnek Sistem Tasarımı”, Journal Of Technical Sciences Volume 8, Issue 2, 25-39.

Krokida, M. K., Maroulis, Z. B., & Saravacos, G. D. (2001), “The effect of the method of drying on the colour of dehydrated products”, International Journal of Food Science & Technology 36(1): 53–59.

Kuzmin, D., 2004, “Introduction to Computational Fluid Dynamics”, Institute of Applied Mathematics, University of Dortmund.

Labrehberi.Com/Unb-400-Etuv-Memmert.

Leblebicioğlu, E., 2019, “What is CFD?”, muhendistan.com, Engineering Courses.

Lee, J., Lee, Y., Choe. E., 2016, “Temperature dependence of the autoxidationand antioxidants of soybean, sunflower, and olive oil”, 10.1007/s00217-006-0532-5.

Lee, M., Chou, L. and Huang, J. 1994. The effect of salt on the surface evaporation of a porous medium, Drying ‘94, Proceedings of the 9th International Drying Symposium, Gold Coast, p. 223.

Li, C.D., Duan, Z.C., Chen, Q., Chen, Z.F., Boafo, F.E., Wu, W.P., Zhou, J.M., 2013, “The effect of drying condition of glassfibre core material on the thermal conductivity of vacuum insulation panel”, Materials and Design 50, 1030–1037.

Makinecim.Com/Bilgi_8147_Kurutma-Ve-Kurutucular-Cesitleri.

Manjarres-Pinzon, K., Cortes-Rodriguez, M., & Rodríguez-Sandoval, E. (2013), “Effect of drying conditions on the physical properties of impregnated orange peel”, Brazilian Journal of Chemical Engineering, 30(3), 667-676.

Mathioulakis, E., Karathanos, V.T., Belessiotis, V.G., 1998. Simulation Of Air Movement in A Dryer By Computational Fluid Dynamics: Application For The Drying Of Fruits. Journal Of Food Engineering 36(2):183–200.

Megep, 2012, “Gıda Teknolojisi, Sebzeleri Kurutma”, P:12-22

Mertoglu, O., 2021, “Geothermal Developments And Projections In Turkey”, International Geothermal Conference.

Midilli, A., Kucuk, H., 2003, “Mathematical Modeling Of Thin Layer Drying Of Pistachio By Using Solar Energy. Energy Conversion And Management”, 44 (7): 1111-1122.

Midilli, A., Kucuk, H., Yapar, Z., 2002, “A New Model For Sıngle-Layer Drying”, An International Journal, Volume 20, Pages 1503-1513.

Milwaukeeinstruments.com/milwaukee-MW102-pro-ph-meter-with-temperature-probe/

Mirade, P.S., Daudin, J.D., 2000. A Numerical Study Of The Airflow Patterns İn A Sausage Dryer. Drying Technology 18(1–2): 81–97.

Moghanaki, S.K., Khoshandam, B., Mirhaj, B.M., “Calculation Of Moisture Content And Drying Rate During Microwave Drying”.

Moisturecontrol.Weebly.Com/Drying-Curve.Html.

Nath, A., Deka, B.C., Mahanta, C.L., 2011, “Thin Layer Drying Of Tomato Slices, Manashi Das Purkayastha”.

Neikov, O.D., 2019, “Handbook Of Non-Ferrous Metal Powders (Second Edition)”.

Netinbag.Com/Tr/Manufacturing/What-İs-A-Drum-Dryer.Html.

Nzifst.Org.Nz/Resources/Unitoperations/Drying5.Htm.

Oluk, C.A., Akyıldız, A., Ağçam, E., Keles, D., Ata, A., 2012, “Farklı Domates Çesitlerinin Bazı Kalite Özellikleri”.

Onwude, D.I., Hashim, N., et. al., 2016, “Modeling the Thin-Layer Drying of Fruits and Vegetables: A Review”.

Ozen, E., Kar, F., 2018, “Farklı Teknikler Kullanılarak Domatesin Kurutulması”, Science and Eng. J of Fırat Univ. 30(1), 47-57, 2018 30(1), 47-57.

Ozgen, F. 2014. “Design of Convective Drying System Used in Apple Drying”, Vol 55, No 656, P. 42-49.

Ozler, S., Tarhan, S., Ergüneş, G., 2004, “Kurutulmuş Cine-Tarım sebzeler”, (http://www.cine- tarim.com.tr/dergi/arsiv62/sektorel03.htm).

Pardeshi, I. L., Arora, S., Borker, P. A., 2009, “ Thin-Layer Drying of Green Peas and Selection of a Suitable Thin-Layer Drying Model”, pages 288-295.

Parikh, D.M., 2014, “Solids Drying: Basics and Applications”.

Popovska – Vasilevska, S., 2003, “Dryıng Of Agrıcultural Products Wıth Geothermal Energy”, St. Kliment Ohridski University, Faculty Of Technical Sciences – Bitola.

Process-Heating.Com/Articles/86586-The-Drying-Curve-Part-1.

Process-Heating.Com/Articles/86587-The-Drying-Curve-Part-2.

Purkayastha, M., Nath, A., Deka, B.C., Mahanta,C.L., 2013, “Thin Layer Drying Of Tomato Slices”.

Rajkumar, R., Kailappan, R., Viswanathan, R., 2007, Foam Mat Drying of Alphonso Mango Pulp”, Drying Technology 25(2):357-365.

Rıchardson, J.F., Backhurst, J.R., 2002, Drying in Chemical Engineering (Fifth Edition), Volume 2.

Richter, A., 2022, “Thinkgeoenergy’s Top 10 Geothermal Countries 2021 – İnstalled Power Generation Capacity (Mwe)”.

Romdhanaa, H., Bonazzia, C., Esteban-Declouxa, M., 2015, “Superheated Steam Drying: An Overview of Pilot and Industrial Dryers with a Focus on Energy Efficiency”, AgroParisTech and INRA, UMR1145 Ingénierie Procédés Aliments, Massy, France.

Sacilik, K., Keskin, R., Elicin, A.K., 2006, “Mathematical Modelling Of Solar Tunnel Drying Of Thin Layer Organic Tomato”, Journal Of Food Engineering, Volume 73, Issue 3, Pages 231-238.

Sahin, F.H., 2010, “Effects of Different Drying Techniques on Some Nutritional Components of Tomato”, Journal of Agricultural Machinery Science, 6(1), 71-78.

Saygı, B., 2019, “Domatesteki Mucizeleri Keşfedin”, Gıda Teknolojileri Elektronik Dergisi.

Senkeser , H., 2018, “Renk Ve Boyar Madde Nedir?”.

Sharifian, F., Modarres-Motlagh, A., Komarizade, M. H., & Nikbakht, A. M. (2013), “Colour change analysis of fig fruit during microwave drying”, International journal of food engineering, 9(1), 107-114.

Sokhansanj, S., Jayas, D.S., 2006, “Drying of Foodstuffs. Handbook of Industrial Drying (3. Edition)”, Edited by S.Mujumdar, A.S. Boca Raton, FL: CRC Press.

Stegou – Sagia, A., Fragkou, D.V., 2015, “Influence Of Dryıng Condıtıons And Mathematıcal Models On The Dryıng Curves And The Moısture Dıffusıvıty Of Mushrooms”, Journal of Thermal Engineering Yildiz Technical University Press, Istanbul, Turkey Vol. 1, No. 4, pp. 236-244.

Sunagritohumculuk.Com/Urun/Domates-Rio-Grande.

Süfer, O., Kumcuoğlu, S., Tavman, S., 2016, “Gıda Mühendisliğinde Hesaplamalı Akışkanlar Dinamiği Uygulamaları”, Akademik Gıda 14(4) 465-471.

Taheri-Garavand, A., Rafiee, S., Keyhani, A., 2011, “Mathematical Modeling Of Thin Layer Drying Kinetics Of Tomato Influence Of Air Dryer Conditions”.

Tan, G., “Drying Systems Used In The Food Industry”, Özel Erzurum Bilim Teknik Ve İnovasyon Koleji, Yakutiye, Erzurum P:20-33.

Tarım Ürünleri Piyasaları, 2021, “Domates” .

Tatar, M., Pirinç, V., 2017, “Potential Of Industrial Tomato Production Of Southeast Anatolian Region İn Turkey”, Iğdır Üni. Fen Bilimleri Enst. Der. / Iğdır Univ. J. Inst. Sci. & Tech. 7(2): 11-20.

The Efficient Use Of Energy (Second Edition), 1982.

Traub, S., Schmidt, U., 2002, “An Experimental Test of Loss Aversion. Journal of Risk and Uncertainty”, 25, 233-249.

Treco.co.uk, 2016.

Treybal, R. E. 1981. Mass Transfer Operations, 3rd edition. McGraw-Hill, Singapore.

TUIK 2021, https://www.tuik.gov.tr/

Tülek, Y., 2016 “Güneşte Kurutulmuş Bamyaların Rehidrasyon Kinetiği Engin Demiray”.

Uludağ İhracatçı Birlikleri Genel Sekreterliği Ar&Ge Şubesi, 2017, “Domates Raporu”.

Villa-Corrales, L., et al. (2010) Numerical and Experimental Analysis of Heat and Moisture Transfer during Drying of Ataulfo Mango. Journal of Food Engineering, 98, 198-206.

Yagcıoglu, A., Demir, V., Gunhan T., 2007, " Effective Moisture Diffusivity Estimation from Drying Data", 3 (4), 249-256.

Zadin, V., et al. (2015) Application of Multiphysics and Multiscale Simulations to Optimize Industrial Wood Drying Kilns. Applied Mathematics and Computation, 267, 465-475.

Zaini, M.A.A., 2010, Dryıng, Chapter 6.

Zielinska, M., & Markowski, M. (2012), "Color characteristics of carrots: effect of drying and rehydration", International Journal of Food Properties, 15(2), 450-466.